Long-term observations of Alaska Coastal Current in the northern Gulf of Alaska

6 authors, including:

Regular article

Long-term observations of Alaska Coastal Current in the northern Gulf of Alaska ☆

Phyllis J. Stabeno [a,*], Shaun Bell [a,b], Wei Cheng [a,b], Seth Danielson [c], Nancy B. Kachel [a,b], Calvin W. Mordy [a,b]

[a] NOAA/Pacific Marine Environmental Laboratory, 7600 Sand Point Way NE, Seattle, WA 98115-6349, USA
[b] Joint Institute for the Study of the Atmosphere and Oceans, University of Washington, Box 354235, Seattle, WA 98195-4235, USA
[c] Institute of Marine Science, University of Alaska, 112 O'Neill, Box 757220, Fairbanks, AK 99775-7220, USA

ARTICLE INFO

ABSTRACT

The Alaska Coastal Current is a continuous, well-defined system extending for ∼1700 km along the coast of Alaska from Seward, Alaska to Samalga Pass in the Aleutian Islands. The currents in this region are examined using data collected at > 20 mooring sites and from > 400 satellite-tracked drifters. While not continuous, the mooring data span a 30 year period (1984–2014). Using current meter data collected at a dozen mooring sites spread over four lines (Seward, Gore Point, Kennedy and Stevenson Entrances, and the exit to Shelikof Strait) total transport was calculated. Transport was significantly correlated with alongshore winds, although the correlation at the Seward Line was weak. The largest mean transport in the Alaska Coastal Current occurred at Gore Point ($1.4 \times 10^6 \text{ m}^3 \text{ s}^{-1}$ in winter and $0.6 \times 10^6 \text{ m}^3 \text{ s}^{-1}$ in summer), with the transport at the exit to Shelikof Strait ($1.3 \times 10^6 \text{ m}^3 \text{ s}^{-1}$ in winter and $0.6 \times 10^6 \text{ m}^3 \text{ s}^{-1}$ in summer) only slightly less. The transport was modified at the Seward Line in late summer and fall by frontal undulations associated with strong river discharge that enters onto the shelf at that time of year. The interaction of the Alaska Coastal Current and tidal currents with shallow banks in the vicinity of Kodiak Archipeligo and in Kennedy–Stevenson Entrance results in mixing and prolonged primary production throughout the summer.

© 2016 Published by Elsevier Ltd.

1. Introduction

The northern Gulf of Alaska (GOA) is an ecosystem dominated by advection, with the well-defined Alaska Coastal Current (ACC) transporting ∼$1 \times 10^6 \text{ m}^3 \text{ s}^{-1}$ anti-clockwise along the coast (Royer, 1982; Stabeno et al., 2004; Weingartner et al., 2005). The ACC is driven by along-shore winds, with a hydrographic signature that is characterized by a low salinity core along the coast. This core results from river runoff, which is confined to the coast by downwelling-favorable winds. Along the shelf break, the slope and basin circulation is dominated by the cyclonic subarctic Alaska Gyre, which consists of the northward flowing Alaska Current, an eastern boundary current, and southwestward flowing Alaskan Stream, a western boundary current (Favorite and Ingraham, 1977).

While an ACC-type current exists along much of the North American coast from Vancouver Island to the arctic (Carmack et al., in preparation), it is not a continuous feature (Stabeno et al., 2016).

Some of these disruptions in the coastal flow are caused by deep submarine canyons, such as at Cross Sound, which cut across the entirety of the shelf. Others are caused by lack of downwelling favorable winds such as occurs between Cross Sound and Yakutat Bay (Stabeno et al., 2004, 2016). The focus of this manuscript is the region from the Kenai Peninsula to Samalga Pass. In this region, the ACC is largely continuous, although it can be interrupted for short periods of time (days) by gap winds (Ladd et al., 2016) and upwelling favorable winds (Stabeno et al., 2004). In addition, it interacts with bathymetry (e.g. troughs, canyons, banks) which both divert water to the slope and introduce slope water onto the shelf (Ladd et al., 2005a).

While from May to August there can be episodes of upwelling, downwelling dominates the northern GOA most of the year (Stabeno et al., 2004). In spite of this dominance of downwelling-favorable winds, high productivity occurs in the northern coastal GOA. Nutrients are supplied to the northern GOA shelf through several mechanisms including: advection, particularly associated with canyons; the relaxation of summer downwelling winds (Childers et al., 2005; Ladd et al., 2005a); estuarine circulation (Stabeno et al., 2004); sediment resuspension; river discharge (Royer and Grosch, 2007); and, during winter, Ekman transport of
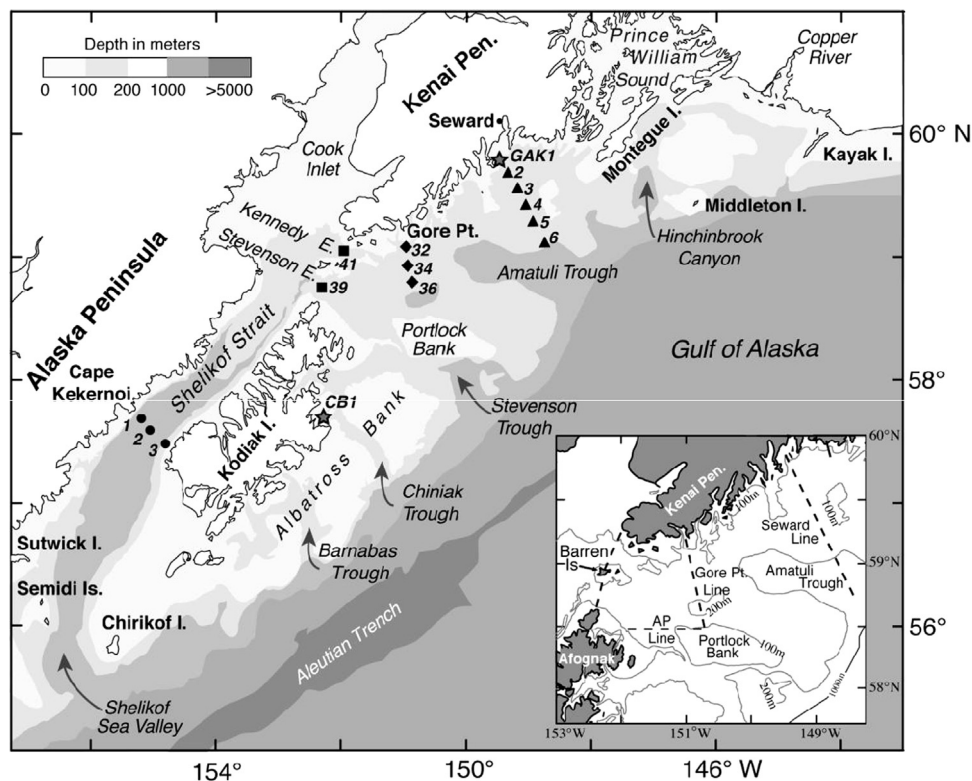
Fig. 1. Map of the coastal Gulf of Alaska from Kayak Island to the exit of Shelikof Strait. Mooring locations are indicated by names or numbers. The inset shows the primary hydrographic lines along the Kenai Peninsula. The hydrographic line at Cape Kekurnoi coincides with the moorings there and is referred to as Line 8. The star on the east side of Kodiak Island is the long-term mooring site CB1, and the one on the Seward line is GAK1. The inset shows the Seward Line (GAK), and the Gore Point (GP), Kennedy–Stevenson (KE–SE), and Afognak–Portlock (AP) lines.

surface water from the central GOA basin onto the shelf (Stabeno et al., 2004). Collectively, these physical processes support enhanced primary and secondary production during the spring and summer (Strom et al., 2007; Coyle et al., 2012, 2013; Stabeno et al., 2004).

The GOA's pelagic production supports some of the nation's largest fisheries and vast numbers of birds and mammals. The region around Kodiak Island (Fig. 1) is of particular importance as a habitat for numerous economically and ecologically important fishes including walleye pollock (Brodeur and Wilson, 1996), Pacific cod (Abookrie et al., 2005), juvenile Pacific halibut, arrowtooth flounder (Meuter and Norcross, 2002) and capelin (Doyle et al., 2002). Kodiak Island is the site of major haul-out and rookery areas for Steller sea lions. Its nearshore region and adjacent troughs support an abundance of juvenile and adult walleye pollock (Wilson, 2000; Hollowed et al., 2007).

Since the early 1980s, multiple papers have been published describing the ACC in the northern GOA – its properties, seasonal variability and dynamics (e.g. Royer, 1981; Reed and Schumacher, 1986; Schumacher et al., 1989; Stabeno et al., 1995, 2004; Weingartner et al., 2005). Most of the papers concentrated on the long-term, hydrographic transect at Seward and those in Shelikof Sea Valley and Strait. These hydrographic data were often used to estimate the geostrophic velocity in the ACC. In 1984, the first arrays of moorings measuring current velocity were deployed in Shelikof Strait and Sea Valley providing estimates of total transport (Schumacher et al., 1989). In the 1990s mooring arrays measuring currents expanded to include Gore Point and Kennedy–Stevenson Entrances (Stabeno et al., 1995). With the deployment of a moored array of current meters on the Seward Line in 2001–2004, four lines existed at which transport could be calculated (Fig. 1). These four cross-shelf mooring arrays were deployed as parts of several large ecosystem studies, including the US GLOBal Ocean

ECosystems Dynamics (GLOBEC) Northern Gulf of Alaska program (2001–2005) and the more recent North Pacific Research Board (NPRB) Gulf of Alaska Integrated Ecosystem Research Project (2011–2014).

Most of the moorings in the northern GOA have been deployed intermittently. Only two of the mooring sites (Fig. 1) have been maintained nearly continuously for more than a decade – GAK1 (since 1998) and CB1 (since 1999). The GAK1 mooring records water properties at multiple depths, while CB1 measures both currents and water properties, but only near the bottom.

In this paper we integrate time series from 16 mooring sites (a total of 169 deployments distributed on four mooring array lines listed in Table 1 and Fig. 2) and >400 satellite-tracked drifters, along with model simulations, to explore the temporal and spatial variability in the ACC from Seward to Cape Kekurnoi, including the differences between the cold "season" (October–April) and the warm "season" (May–September), spatial coherence and the relationship to winds. This large data set, together with other published results, permits the development of a schematic of the transports in ACC during the warm and cold seasons from Seward, Alaska to the eastern Aleutian Passes.

2. Methods

2.1. Winds

Reanalysis data was obtained from the North American Regional Reanalysis (NARR) and from the National Centers for Environmental Prediction Reanalysis 2 (NCEPR2) for the North American Region. NARR uses the high resolution NCEP Eta model (~32 km grid size compared to NCEPR2's 2.5° grid) and includes additional assimilated parameters to improve the reanalysis

Table 1
Statistics on transport measured at the four GOA lines: Shelikof Strait, Kennedy–Stevenson Entrances, Gore Point and the Seward Line. The shaded area in the first column indicates the winter period. Correlations are with NARR winds, with a positive lag indicating that the winds lead the transport. For two periods (14 January–12 July 1985, and 10 May–15 July 1989) transport was calculated from moorings in Shelikof Sea Valley not at the exit to Shelikof Strait, so there is no upstream calculation made.

Start Date	# of 6 h points	Correlation	Lag (days)	95% Sig. Level	Mean Transport (10^6 m^3 s^{-1})
Shelikof Strait – 3 moorings					
Aug. 27, 1984	75	0.67	0.50	0.37	0.31 (0.66)
May 10, 1985	288	0.58	0.50	0.27	0.57
May 10, 1989	256	0.49	0.50	0.21	0.38
May 10, 1991	486	0.49	0.75	0.17	0.54 (0.82)
May 10, 1996	510	0.47	0.50	0.18	0.06 (0.34)
May 10, 1998	486	0.49	0.50	0.21	0.21 (0.47)
May 15, 2001	486	0.48	0.75	0.18	0.29 (0.58)
May 15, 2002	400	0.45	0.75	0.20	0.21 (0.44)
May 10, 2003	460	0.47	0.25	0.18	0.42 (0.63)
May 23, 2004	468	0.27	0.5	0.17	0.09 (0.39)
May 10, 2005	512	0.45	1.00	0.19	0.39 (0.58)
Oct. 1, 1984+	810 (416)	0.62	0.50	0.14	1.02 (1.32)
Mar. 16, 1996	150	0.59	0.75	0.32	0.77 (1.06)
Feb. 21, 1998	240	0.45	4.5	0.25	0.83 (1.18)
Oct. 1, 2001	378	0.55	0.5	0.28	1.23 (1.55)
Jan 17, 2002	384	0.37	0.5	0.17	0.88 (0.99)
Mar. 3, 2003	200	0.65	0.50	0.36	1.12 (1.49)
Oct.1, 2004	810	0.52	0.50	0.17	0.91 (1.25)
Oct. 1, 2005	240	0.55	0.50	0.22	1.07 (1.40)
Kennedy–Stevenson – 2 moorings (3 in 1991)					
May 10, 1991	512	0.54	0.75	0.15	0.43
May 10, 2011	512	0.70	0.75	0.28	0.56
May 10, 2013	512	0.38	0.75	0.16	0.21
Gore Point – 3 moorings (7 in 1991)					
June 1, 1991	420	0.60	0.75	0.18	0.74
May 10, 1994	504	0.60	0.50	0.19	0.62
May 13, 2001	486	0.46	0.50	0.17	0.57
May 28, 2002	432	0.44	0.75	0.18	0.39
May 10, 2003	500	0.45	0.75	0.14	0.59
May 10, 2004	324	0.63	0.75	0.24	0.41
May 10, 2011	500	0.65	0.50	0.25	0.44
May 10, 2013	504	0.41	0.50	0.15	0.89
Oct. 1, 2001	400	0.42	0.75	0.23	1.50
Oct. 1, 2002	810	0.43	0.75	0.12	1.30
Oct. 1, 2003	810	0.46	0.75	0.13	1.31
Oct. 1, 2013	360	0.45	0.75	0.15	1.39
Seward Line – 3 or 4 moorings					
May 16, 2001	486	0.24	0.50	0.16	0.36
May 28, 2002	447	0.19	0.50	0.14	0.49
May 10, 2003	512	0.21	0.50	0.14	0.46
May 10, 2004	326	0.21	0.50	0.16	0.35
Oct. 1, 2001	160	0.31	2.0	0.23	0.81

product (Mesinger et al., 2006). NCEPR2 output is compared to the NARR output. Reanalysis estimates of winds are available at 3-h intervals for NARR and 6-h intervals for NCEPR2. Both data sets were binned and averaged into 12-h intervals. The NCEPR2 and NARR data were provided by the NOAA/OAR/ESRL PSD, Boulder, Colorado, USA, from their web site at http://www.esrl.noaa.gov/psd/.

Wind velocity was measured on a series of surface moorings deployed on the Seward Line at GAK5 (2001–2004). Mooring winds were measured ~3 m above the ocean surface and are adjusted to the reanalysis height of 10 m assuming a power law wind profile and neutral stability (Hsu et al., 1994). All moored meteorological equipment (Coastal Environmental's WeatherPAK 2000 with an R/M Young Anemometer and Eppley PSP Radiometer) was prepared and data processed according manufacturers' specification. Data were collected hourly and averaged into two bins: 00:00–12:00 GMT and 12:00–24:00 GMT for comparison with reanalysis data.

Moorings were deployed in spring and replaced in late summer or early fall. While the spring-summer equipment functioned well, the anemometers generally failed in late fall due to the high wind speeds that occur each fall at the site. In winter 2003, the entire surface toroid was lost, although the oceanographic equipment was recovered from the sea floor in the spring.

2.2. Moorings

This paper focuses on currents and water column measurements (temperature, salinity) made at 16 sites (Figs. 1 and 2) during the period from 1984 to 2014. Subsurface moorings were all taut-wire, measuring temperature (SeaBird Electronics SBE-37, SBE39, and Aanderaa RCM-9), salinity (SBE-37 and SeaCats), currents (RCM-7, RCM-9 and Teledyne RD Instruments acoustic Doppler current profilers - ADCP). Most of the ADCP moorings consisted of a bottom mounted, upward-looking 150 (prior to 2000), 300 or 75 kHz instruments (2000–2014). The mooring at
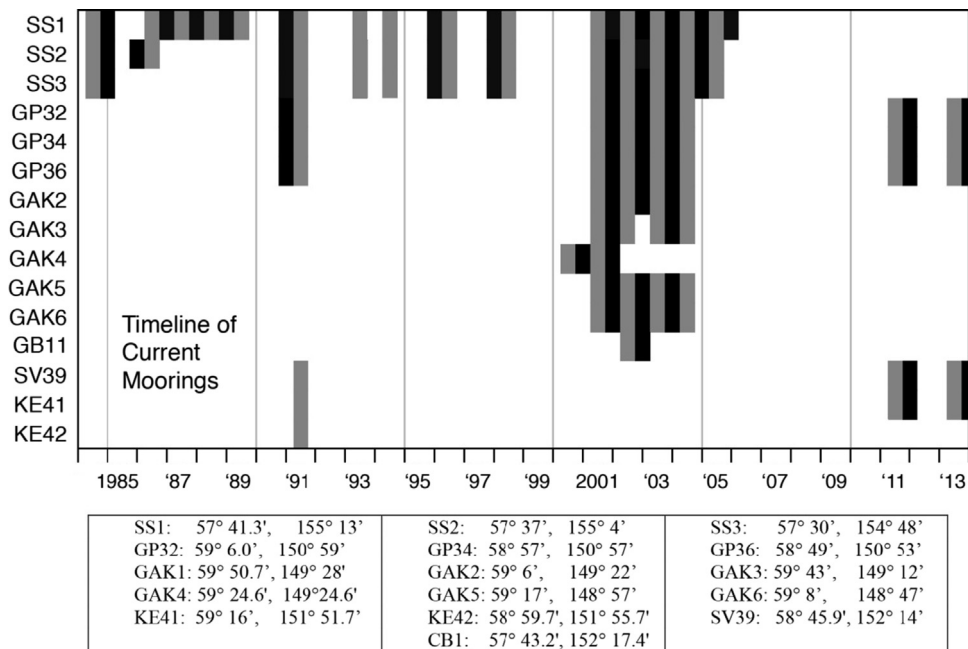
Fig. 2. Time line of moorings on which currents were measured. The files are broken into warm period (May 10–September 15), indicated in gray, and the cold period (October 1–April 25), indicated in black. If there were more than 10 days in a warm or cold period the grid is colored. List of all moorings used and their positions are shown at the bottom. Temperature and salinity were measured on GAK1 (1998–present) and CB1 (1999–present) are included in the list, but not on the time line. The two to three letter codes in mooring names are: SS–Shelikof Strait; GP – Gore Point; GAK – the Seward Line; KE – Kennedy Entrance; SV – Stevenson Entrance; and CB – Chiniak Trough. GAK1 and GAK4 were deployed by the University of Alaska, Fairbanks and the remainder by the Pacific Marine Environmental Laboratory.

GAK4 consisted of two 300 kHz ADCPs, both at a depth of $\sim$100 m, one upward-looking and one downward-looking,

All moored oceanographic equipment was prepared and the data processed according to manufacturers' specifications. Sampling on all instruments was at half-hourly or hourly intervals. Temperature and salinity from the moored instruments were compared to available nearby hydrographic casts for calibration.

Transport was calculated at each of the four lines (Shelikof Strait, Kennedy–Stevenson Entrance, Gore Point and Seward lines; Fig. 1). Time series of the velocity component normal to the mooring line were used to compute the transport through a section following Schumacher et al. (1989). The normal component of velocity was low-pass filtered with a 35-h, cosine-squared, tapered Lanczos filter. This component of velocity at each current meter or ADCP bin was then multiplied by the cross-sectional areas. The horizontal boundaries of cross sectional areas were defined as the halfway line between moorings, or to the land, as appropriate. On the outer edge of the mooring line at Gore Point and Seward, the edge was defined as the same half-distance as between the outer mooring and its nearest more coastal neighbor. The vertical boundaries were the surface, the bottom, or the halfway point between instruments, as appropriate. These time series were then summed, providing a time series of transport perpendicular to the mooring line. This method was successfully employed previously to obtain time series of transport in Shelikof Strait (Stabeno et al., 1995), Gore Point (Stabeno et al., 1995) and the Alaskan Stream (Stabeno Hristova, 2014).

Transport in Shelikof Strait (SS) were calculated using current measurements at SS1, SS2 and SS3 except from 15 January 1985 to 1 May 1985 and in 1989. During both periods, the transport was calculated using mooring arrays in the sea valley not at the exit of the Strait (Schumaher et al., 1989; Stabeno et al., 2004).

Unless otherwise noted, the current, temperature and salinity time series presented here were low-pass filtered with a 35-h, cosine-squared, tapered Lanczos filter to remove tidal and higher-frequency variability. The time series were then re-sampled at 6-h intervals.

2.3. Satellite-tracked drifters

Since 1986, $>$ 400 satellite-tracked drifters (drogue centered at $\sim$40 m) have been deployed in the North Pacific by investigators from the EcoFOCI program at Pacific Marine Environmental Laboratory (www.ecofoci.noaa.gov/drifters/efoci_driftersIntro.shtml). During 1986–1988, "holey sock" drogues were used, between 1987 and 1993, "tristar" drogues were employed, and since 1994 "holey sock" drogues have once again been used. At these northern latitudes, an average of $\sim$14 position fixes per day were obtained from Argos. Once the data were received from Argos, the data were quality controlled. Data were deleted from the time series following loss of the drogue. The resulting position time series were then linearly interpolated to hourly intervals.

Lagrangian velocities were determined by centered differences from the hourly drifter positions. A low-pass filter (24 h running mean) was applied to the drifter data. The methods used in deriving mean velocities are described by Stabeno and Reed (1994). Data were gridded into cells of 0.25° latitude by 0.5° longitude ($\sim$25 km $\times$ 25 km). In the northern GOA, the integral time scale for velocity (Kundu and Allen, 1976) was 1–3 days. Noting this, all measurements in a grid cell within a 3-day period were averaged together providing a set of independent estimate associated with that grid cell. Finally, if the derived scalar speed was less than the standard error, or there were fewer than five independent estimates, mean velocities were not considered sufficiently robust to be included. Lagrangian velocity is particularly useful in revealing spatial patterns of flow, but is not directly comparable to the Eulerian (from current meters) velocities.

2.4. Model description

The Regional Ocean Modeling System (ROMS) version 3.0 is a hydrostatic, primitive equation, generalized sigma-coordinate model. A full description of ROMS can be found in Haidvogel et al. (2000, 2008), Shchepetkin and McWilliams (1998, 2003, 2005), and references therein. ROMS has been implemented on a

series of grids with increasing horizontal resolution in the North Pacific Ocean (Curchitser et al., 2005; Hermann et al., 2009a, 2009b). The particular grid used for this study has 3-km horizontal resolution and covers the entire GOA (Cheng et al., 2012). It has 42 levels vertically. Vertical tracer and momentum mixing is parameterized using the K-profile parameterization scheme (Large et al., 1994), which includes both a surface and a bottom boundary layer (Durski et al., 2004). The ROMS grid is oriented such that its "eastern" and "northern" boundaries are against the land mass, while its "southern" (intersects coast at ~52°N) and "western" (intersects the Alaska Peninsula at ~164°W) boundaries are open, allowing entry and exit of the Alaskan Stream and the exit of ACC (see Fig. 1 in Cheng et al., 2012). Tracer and 3-D momentum fields from Simple Ocean Data Assimilation (SODA; Carton and Geise, 2008) at the open boundaries are treated with a radiative boundary condition with adaptive nudging as described by Marchesiello et al. (2001). The Chapman scheme is used for sea surface height (Chapman, 1985), and the Flather scheme is used for barotropic velocities (Flather, 1976).

Additionally, tidal forcing obtained from Foreman et al. (2000) is applied at the open boundaries. Four diurnal (O1, Q1, P1, and K1) and four semidiurnal (N2, S2, K2, and M2) tidal constituents are used. ROMS is driven by sea surface heat and momentum fluxes calculated using bulk algorithms (Fairall et al., 1996) given the time dependent atmospheric forcing and modeled sea surface temperature (SST). The atmospheric forcing is taken from Version 2 forcing for Common Ocean-ice Reference Experiments (CORE2) (http://data1.gfdl.noaa.gov/nomads/forms/mom4/COREv2.html). Forcing variables include sub-daily surface winds, sea level pressure, surface air temperature and specific humidity, precipitation, and radiation fluxes. The model is also driven by monthly estimates of freshwater runoff along the Alaskan coast. The runoff forcing is constructed by combining the mean spatial pattern of global runoff in Dai and Trenberth (2002) with the spatially integrated monthly runoff estimates of Royer and Grosch (2007) and Royer (personal communication); note these include all major rivers in the GOA, as well as distributed sources. The runoff is applied as freshening of the topmost model layer near the coast. Total runoff along each segment of coastline is distributed using an exponential taper based on distance squared from the coastal point to the interior of the ocean, with an e-folding scale of 30 km.

ROMS was initialized on January 10, 2000 based on the SODA products, and the model was run continuously through October 2005. Daily, tidally-filtered averages were saved for subsequent analyses.

3. Results and discussion

3.1. Winds

NCEP's Reanalysis product Version 2 (NCEPR2; Kalnay et al., 1996) has long been the standard for atmospheric forcing data in oceanographic studies, especially when few direct observations are available. Previous studies have discussed the quality of the reanalyis as it pertains to the northeast Pacific. The influence of topography is not well resolved around coastal locations in the NCEPR2 Reanalysis data resulting in a need for caution when using coastal winds (Ladd and Bond, 2002). This may be even more confounded by complex terrain, such as the steep coastal mountains that occur along the coast in the GOA (Fig. 1). Here, terrain flows such as gap winds have been observed (Ladd et al., 2016). In addition, Shelikof Strait lies between the mountains of the Alaska Peninsula and Kodiak Archepelago, which results in down gradient winds in the Strait (Stabeno et al., 2004).

Since meteorological data collected on the moorings deployed on the Seward line in 2001–2004 were not assimilated into the reanalysis product, they serve as a useful independent measure of reanalysis accuracy. Two years (2001 and 2003) of wind data collected at GAK5 are compared to the corresponding NARR and NCEPR2 winds (Table 2). The region of interest is the northern GOA near the Kenai Peninsula (Fig. 1). Data were collected during May–November 2001 and mid April–mid September 2003. Using the nearest model gridpoint, the NARR comparison location is to the southeast of the mooring location whereas the NCEPR2 comparison location is to the northeast close to the coast. No interpolation was used to account for the variation in locations. The NARR wind velocity components were consistently better correlated ($r^2 = 0.84 - 0.91$) to the winds measured at GAK5 than those from NCEPR2 winds ($r^2 = 0.71 - 0.81$). NARR winds were also found to be stronger than the NCEPR2 winds, although both across-shore and along-shore components from NARR were still ~15% weaker than the observed winds measured at GAK5 (Fig. 3).

Table 2
Comparison between the observed winds at GAK5 and the modeled NARR and NCEPR2 winds. These are vector correlations, with the angle between the vectors indicated in the 3rd and 5th columns.

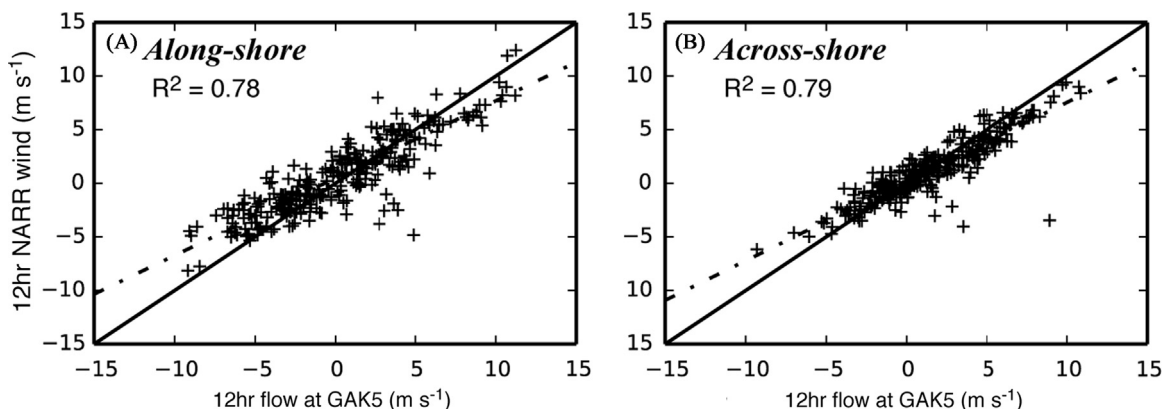| Mooring (GAK5) period sampled	NARR		NCEP-R2	
	Vector correlation	Angle (deg)	Vector correlation	Angle (deg)
2001 Summer	0.84	0	0.71	−19
2001 Fall	0.91	22	0.81	7
2003 Summer	0.90	7	0.76	−15

Fig. 3. Comparison between NARR and measured winds at GAK5 during summer deployment of 2003 (April–September) for (A) alongshore winds and (B) across-shore winds. R^2 values for the linear fits are shown in the top left corner of each plot. These correlations are greater than those with the NCEP2 winds (not shown).
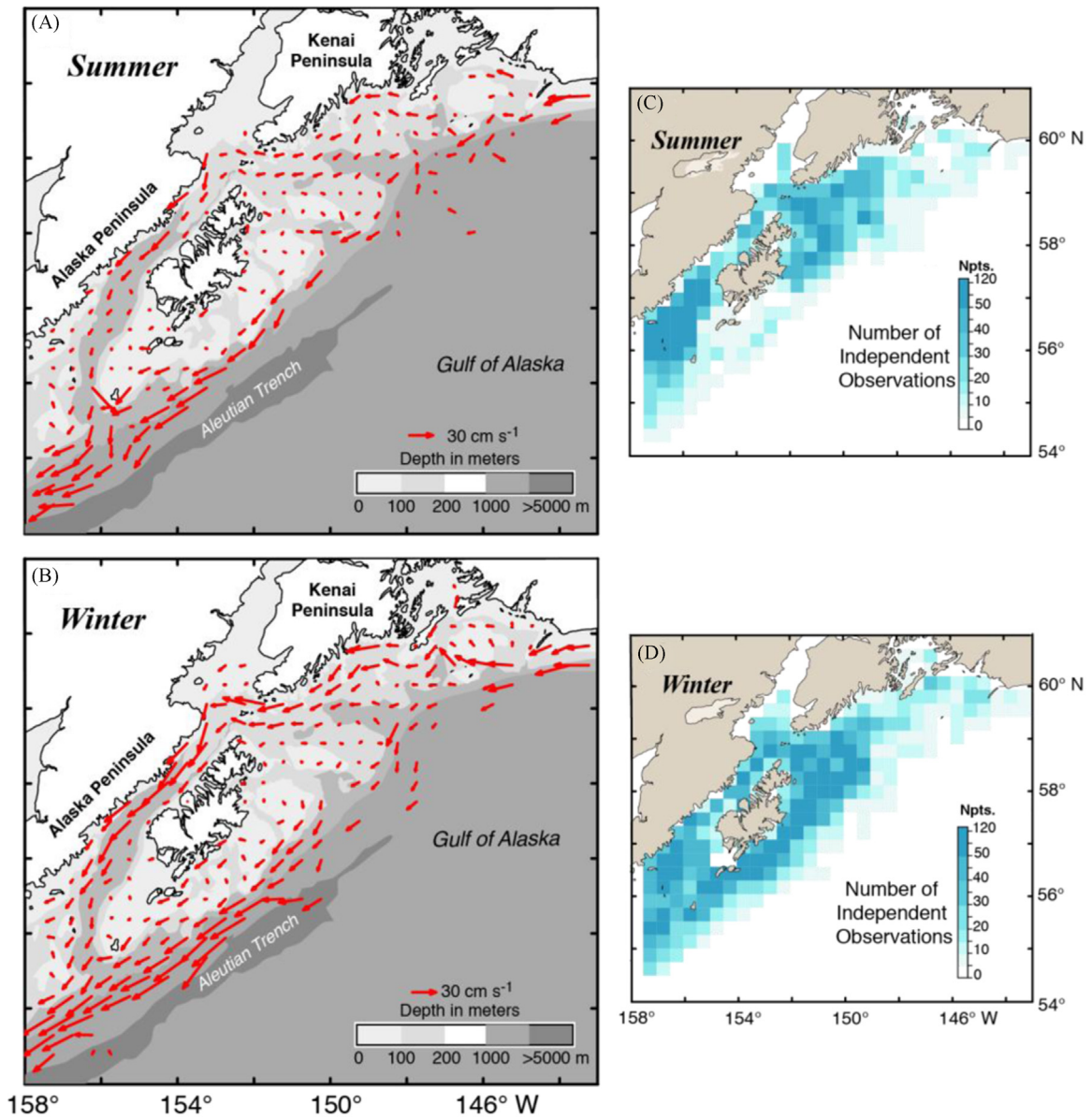
Fig. 4. Maps of currents at ~40 m derived from drifter trajectories for (A) summer and (B) winter. The number of independent estimates for each vector is shown in (C) summer and (D) winter.

3.2. Spatial patterns of flow derived from satellite-tracked drifters and moorings

Mean Lagrangian velocity was calculated for two periods: the warm season (May 10–September 15) and for the cold season (October 1–April 25). Many of the drifters entered into the large eddies found in the basin (Ladd et al., 2005b, 2007) and remained within them for months. These trajectories can dominate the signal. For instance, if an eddy remains nearly stationary for 90 days, which is not uncommon, and the drifter remains within the eddy for that period, then that single event contributes 30 data points to the average overwhelming the derived pattern of non-eddy currents. The mean velocities shown here have excluded trajectories of drifters caught in an eddy from the analysis.

The large number of drifter trajectories provide information on the spatial patterns of flow (Fig. 4). The best coverage occurs to the west of the Seward line (Fig. 4C, D). In general, the currents on the shelf were stronger in the winter than the summer, but many of the patterns were similar in the two "seasons." On the shelf from Yakutat Bay to Kayak Island, drifters were advected westward

(Stabeno et al., 2016). Both the cold and warm seasons showed an interruption of the coastal flow at Kayak Island (Fig. 4). Most of the drifters were transported off the shelf onto the slope at Kayak Island, requiring the ACC to reform along the coast somewhere east of Kayak Island. West of the island, the flow was weak near the coast, but on the outer shelf, there was onshelf flow especially during "winter" (Fig. 4A, B). The drifter composites showed the ACC began to reform along Montague Island and is well formed at Seward. A similar pattern is evident in model runs (see Fig. 2 in Wang et al., 2014). Of the 8 drifters advected into the vicinity of Hinchinbrook Entrance, only one entered Prince William Sound. Recent analysis of 40 years of hydrographic data suggests that the Prince William Sound flow field is likely subject to significant inter-seasonal and inter-annual variability (Musgrave et al., 2013). During winter, the strong downwelling favorable winds force surface water, including the Copper River plume, through Hinchinbrook Entrance, while during summer, with the relaxation of downwelling favorable winds, the more dense deeper water flows over the Hinchinbrook sill into Prince William Sound (Niebauer et al., 1994).

West of Prince William Sound, the flow continued southwestward along the Kenai Peninsula, and then entered Shelikof Strait through Kennedy and/or Stevenson Entrance. Observations from earlier data sets indicate that ~75% of the ACC, measured at the exit of Shelikof Strait, leaves the shelf via the Shelikof Sea Valley (Schumacher et al., 1989), although onshelf flow is evident in current meter records between the Semidi Islands and Chirikof Island in both summer and winter. The remainder of the ACC continues along the peninsula eventually entering the Bering Sea through Unimak Pass and the other shallow Aleutian Passes east of 170°W (Ladd et al., 2005a; Stabeno et al., 2005; Stabeno and Hristova, 2014).

Onshelf flow is evident in Amatuli Trough and near Hinchinbrook Canyon, but only in the "winter." The influence of the other troughs (Chiniak, Stevenson and Barnabus Troughs) is not evident in the Lagrangian current patterns, because of the relatively large grid scale. Their influence, however, is evident in individual drifter trajectories (e.g. Fig. 8 in Ladd et al., 2005b; Fig. 10 in Stabeno et al., 2004).

The Alaskan Stream is clearly evident along the slope shoreward of the Aleutian Trench (Fig. 4A, B). A well-defined Alaskan Stream appears to form at the mid-point along Kodiak Island. The satellite-tracked drifter trajectories revealed large numbers of mesoscale eddies at the head of the gulf near Amatuli Trough (Ladd et al., 2007). Since data from drifters in eddies were not included in this analysis, there are fewer data points in this region. The recurrence and persistence of eddies in this region is indicative of a poorly formed Alaskan Stream. The Alaskan Stream continues to strengthen as it moves westward, with the largest mean near surface speeds occurring near 164°W (Stabeno and Hristova, 2014). It appears that the near surface flow in the Alaskan Stream was stronger in the winter than summer (Fig. 4), which was also observed farther west at ~170°W (Stabeno and Hristova, 2014).

3.3. Vertical structure and transport derived from moored current meters

The vertical structure of currents, derived from the measurements on the moorings, shows a similar pattern of the ACC at each of the four lines (Figs. 5 and 6), with the strongest currents near the surface along the coast. At all depths, the mean flow at Gore Point and Kennedy–Stevenson Entrances was positive (toward the west) with no reversals, but there was northeastward flow (negative) near the bottom and on the southern side of Shelikof Strait. Along the Seward line, the ACC was strongest at GAK2 and GAK3, and weak at GAK4. The flow at GAK5 was near zero and actually negative (eastward) in the summer, indicating that site was outside the ACC. As expected, the flow in the winter at Gore Point, Shelikof Strait and Seward (there is no winter data at Kennedy–Stevenson Entrances) was stronger than that during the summer months (Figs. 5 and 6).

Mean transports were greatest at Gore Point, ranging from a seasonal average of $0.39–0.89 \times 10^6 \, \mathrm{m^3 \, s^{-1}}$ (average $0.58 \times 10^6 \, \mathrm{m^3 \, s^{-1}}$) in the summer months to $1.30–1.50 \times 10^6 \, \mathrm{m^3 \, s^{-1}}$ (average $1.38 \times 10^6 \, \mathrm{m^3 \, s^{-1}}$) in the winter (Table 1). Mean net transports were weaker at the exit to Shelikof Strait, ranging from 0.06 to $0.57 \times 10^6 \, \mathrm{m^3 \, s^{-1}}$ (average $0.32 \times 10^6 \, \mathrm{m^3 \, s^{-1}}$) in the summer months to $0.77–1.23 \times 10^6 \, \mathrm{m^3 \, s^{-1}}$ (average $0.98 \times 10^6 \, \mathrm{m^3 \, s^{-1}}$) in the winter. The flow in Shelikof is more complex, however, with northeastward inflow typically on southern side of the strait and the southwestward flowing ACC occupying the remainder of the cross section of the strait. Within Shelikof Strait, the inflow is entrained into the ACC. The average inflow is $0.26 \times 10^6 \, \mathrm{m^3 \, s^{-1}}$, in the summer and $0.30 \times 10^6 \, \mathrm{m^3 \, s^{-1}}$ in the winter, which is similar to the measured inflow between Semidi Islands and Chirikov Island (Fig. 1) of $0.2 \times 10^6 \, \mathrm{m^3 \, s^{-1}}$ measured in 1984–1985, the
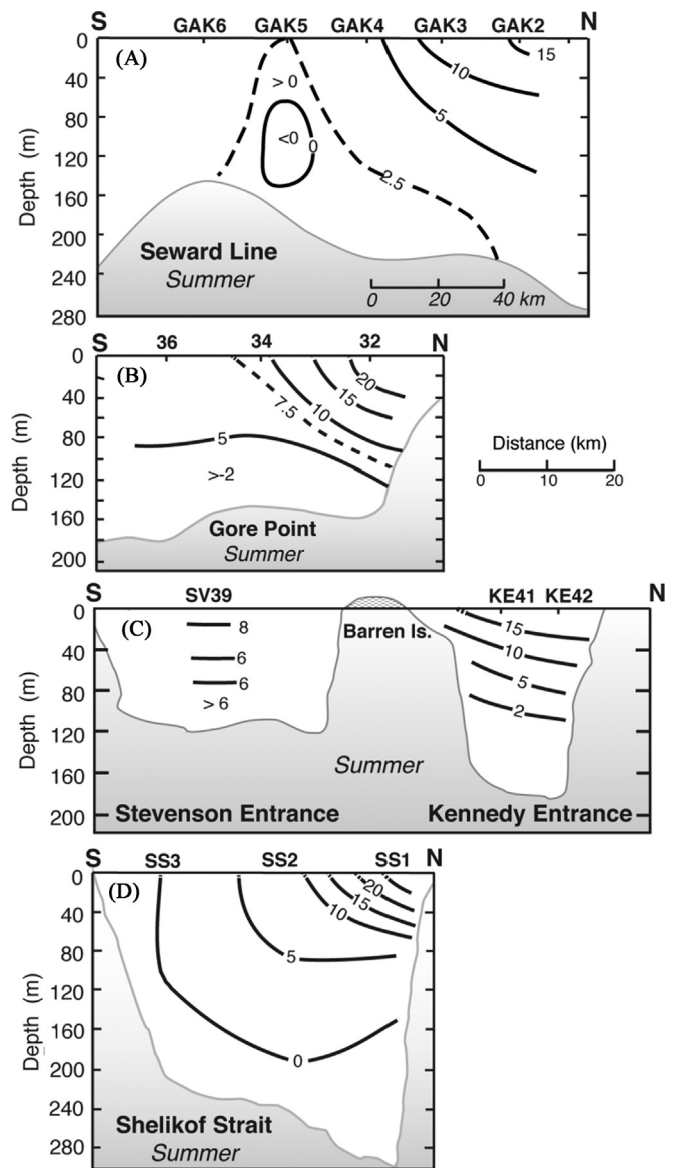

Fig. 5. Cross section of mean currents (cm s^{-1}) perpendicular to the plane of the moorings with positive into the page (westward or southwestward) for summer at (A) the Seward line, (B) Gore Point, (C) Kennedy and Stevenson Entrances and (D) Shelikof Strait. The means were calculated from all available data at the mooring locations indicated in Fig. 2.

single year that there were moorings there. The ACC's average transport (the southwestward flow) is $0.55 \times 10^6 \, \mathrm{m^3 \, s^{-1}}$ in the summer months and $1.28 \times 10^6 \, \mathrm{m^3 \, s^{-1}}$ in the winter months, making the transport at the exit to Shelikof Strait slightly less than that measured at Gore Point. The other two lines (Kennedy–Stevenson Entrances and Seward) have far fewer occupations (Fig. 2), and only one winter occupation; this more limited data set indicated weaker transport than that at Gore Point.

The time series of transport were significantly (95% significance level) correlated to local NARR winds (Table 1), although the weakest correlations consistently occurred between the transport on the Seward Line and the NARR winds. Usually the winds led the transport by 12 or 18 h (the inertial period is ~18 h). In general, the transports at Shelikof Strait, Gore Point and Kennedy–Stevenson were all well correlated and usually in phase (Table 3). In contrast, the correlations between the transports measured at the Seward Line and the transports measured on other lines were at best weakly correlated. This helps define a possible length scale for
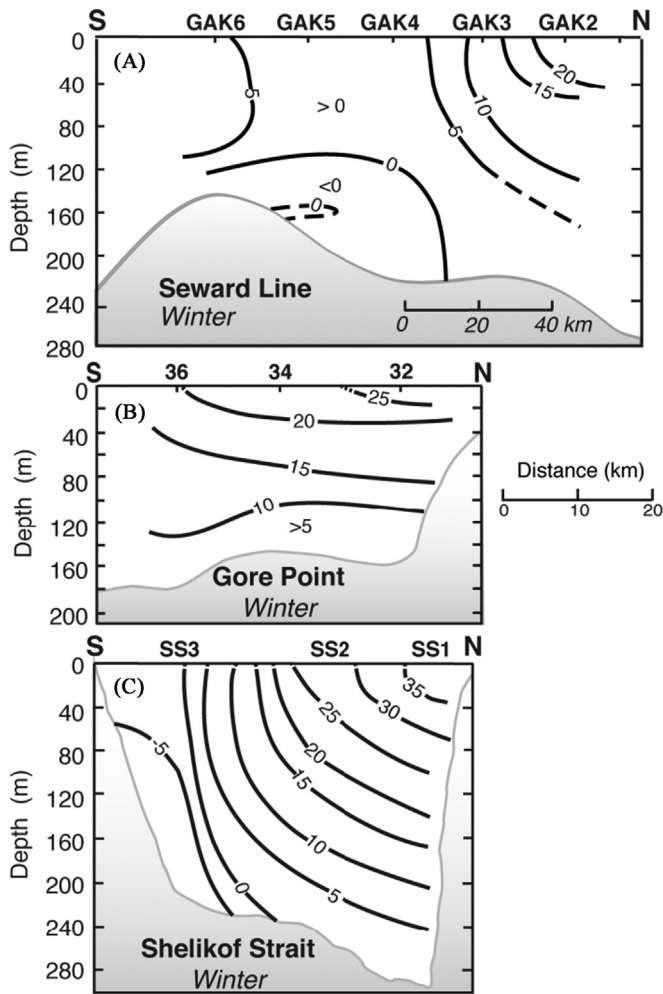
Fig. 6. Cross section of mean currents (cm s^{-1}) perpendicular to the plane of the moorings with positive into the page (westward or southwestward) for winter at (A) the Seward line, (B) Gore Point, and (C) Shelikof Strait. The means were calculated from all available data at the mooring locations indicated in Fig. 2.

the along-shore coherence of the flow. Interestingly, this scale is appreciably shorter than the dominant atmospheric length scales, suggesting the importance of other processes in regulating local flow variations. Possible causes of the weak correlations are discussed in Section 3.4.

There were sufficient occupations at Gore Point and the exit of Shelikof Strait to examine magnitude of seasonal transport fluctuations. To simplify the comparison between the transports at the exit of Shelikof and at Gore Point, we focus on the net transport at the exit Shelikof Strait, not the larger ACC transport there. In 1991, one of the times when there were measurements on both lines, the transport at Gore Point was typically greater than that at Shelikof Strait (Fig. 7A). The variations in transports were similar at the two sites, with high and low (or negative) flow events occurring in phase at the two lines. On multiple occasions, Shelikof Strait transport was northeastward (negative), while at Gore Point the flow weakened (in phase) but did not reverse, suggesting flow around the outer side of Kodiak Island. During periods of negative flow at the exit of Shelikof Strait, there was enhanced northeastward flow along north side of Kodiak Island (Fig. 7B, C), forced by southwesterly winds.

All the time series of transport at Gore Point and Shelikof Strait show similar patterns of flow to those that were observed in 1991 (Fig. 8A, B). Transport was stronger in the winter than summer, with maximum episodic events at Gore Point and in the net

transport at Shelikof Strait exceeding 3×10^6 m^3 s^{-1}. Stronger events ($> 4.5 \times 10^6$ m^3 s^{-1}) occurred when just the ACC transport was considered (Fig. 8C). Throughout the year, although primarily in summer, there were periods of 1–3 days when the net transport in Shelikof was negative; this did not happen at Gore Point. Because of this, the transport time series at Gore Point exhibits lower variance than the net transport at Shelikof Strait. In contrast, the monthly mean transports (Fig. 8E) were consistently greater at Gore Point than the net transport at Shelikof Strait. The transport in the ACC (downstream) was also marginally weaker (except in January) than at Gore Point. Using mean transports derived from Table 1, 55% (0.32×10^6 m^3 s^{-1}/0.58×10^6 m^3 s^{-1}) of the summer transport at Gore Point flowed down Shelikof Strait and 71% (0.98×10^6 m^3 s^{-1}/1.38×10^6 m^3 s^{-1}) of the winter transport flowed down the strait. The remainder must have been diverted to the southeast of Kodiak Island: 0.22×10^6 m^3 s^{-1} in summer and 0.40×10^6 m^3 s^{-1} in winter.

The seasonality of transport in Shelikof Strait is also reflected in the trajectories of the satellite-tracked drifters (Fig. 9). In summer, approximately half the satellite-tracked drifters transiting along the Kenai Peninsula bypassed Kennedy–Stevenson Entrances and moved along the southeast coast of Afognak and Kodiak Islands. In winter, the stronger flow in Shelikof Strait resulted in most of the drifters entering the strait through Kennedy or Stevenson Entrances. This increase in the total percentage of drifters advected down Shelikof Strait resulted from the increased number of drifters transiting through Stevenson Entrance (i.e., a broadening of the ACC).

3.4. Instabilities in the ACC

Mysak et al. (1981) observed low-frequency fluctuations in the southwestwardly flowing ACC in Shelikof Strait. At the northern end of the strait, waves appeared at periods of 2.0–3.5 days, while downstream, at the exit, periods were slightly longer, at 4.4–6.2 days. The wavelength was ~74 km. They attributed these fluctuations to baroclinic instability. Similarly, waves in the coastal plume were also evident along the coast from Copper River to Kenai Peninsula (Fig. 10). The true color image shows sediment, likely originating in the Copper River (Wang et al., 2014), delineating the wave pattern (wavelength ~20 km) along the coast, especially east of the Seward line. Along the Kenai Peninsula, to the west of Seward, there was little evidence of these waves along the coast. Model simulations of salinity at 5 m (Fig. 10C) show a similar, albeit weaker, pattern of waves along the coast east of Seward.

These observed and modeled meanders are clearly evident in the near surface salinity time series at GAK2 and GAK3; there was no evidence of these meanders in the salinity records at Gore Point (GP32 and GP34). There was a similar freshening at GAK1 in August–December, but the variability at frequencies of 2–8 days was not correlated with the variability at GAK2. In 2001, a series of 6 crests could be seen in the cross section of salinity extending ~50 km from the coast (Fig. 11A). The wave was not evident in temperature and appeared to be confined to the upper ~80 m in salinity (Fig. 11B, C). In the model the wave was less distinct - the salinity signal was weaker and had a longer period. The weaker across-shelf gradient in the modeled salinity was likely an artifact of how freshwater was introduced along the coast and enhanced diffusion in the model. This weaker gradient would likely result in the longer period evident in model simulation compared to the observations (Fig. 11A vs. D). The wave was also evident in the currents at GAK2, and to a lesser extent at GAK3, and in the modeled velocity at 10 and 25 km. It would not be expected, however, for the model to reproduce the exact timing of the instabilities.

Table 3

Correlations (r) and the maximum correlation (r-max) among transports at the four GOA lines, along with the lag in days (within 1.5 days) for r-max. The 95% significance level (signif.). Italics indicate the correlation is not significant.

|	Shelikof Strait			Kennedy–Stevenson Ent.			Gore Point		
	r/r-max	signif (95%)	lag (d)	r/r-max	signif. (95%)	lag (d)	r/r-max	signif (95%)	lag (d)
Summer-1991	**11 Apr–1 Oct**			**11 Apr–1 Oct**					
KE&SE	0.81/0.81	0.23	0.00						
Gore Pt.	0.83/0.83	0.24	0.00	0.85/0.85	0.24	0.00			
Summer-2001	**10 May–15 Sep**						**10 May–15 Sep**		
Gore Pt.	0.62/0.62	0.22	0.00						
Seward	0.21/0.30	0.2	0.25				0.10/0.20	0.20	0.50
Summer-2002	**28 May–25 Aug**						**28 May–15 Sep**		
Gore Pt.	0.37/0.37	0.32	0.25						
Seward	0.15/0.17	0.2	0.50				*0.04/0.32*	*0.23*	*1.00*
Summer-2003	**Jul 26–15 Sep**						**Jul 26–15 Sep**		
Gore Pt.	0.72/0.72	0.29	0.00						
Seward	0.57/0.57	0.38	0.00				0.42/0.42	0.26	0.00
Summer-2004	**23 May–30 July**						**23 May–30 July**		
Gore Pt.	0.58/0.60	0.24	0.25						
Seward	− 0.12/0.00	0.18	1.50				0.11/0.24	0.18	1.50
Summer-2011				**01 May–5 Oct**					
Gore Pt.				0.78/0.78	0.41	0.00			
Summer-2013				**04 May–30 Sep**					
Gore Pt.				0.63/0.64	0.28	0.25			
Winter 2001–2002	**1 Oct.'01–4 Jan.'02**						**1 Oct.'01–9 Nov.'01**		
Gore Pt.	0.42/0.50	0.5	0.50						
Seward	0.49/0.49	0.26	0.00				0.30/0.33	0.23	0.00
Winter 2001–2002	**1 Oct.'01–9 Nov.'01**						**1 Oct.'01–9 Nov.'01**		
Gore Pt.	0.50/0.52	0.31	0.25						
Seward	0.49/0.49	0.26	0.00				0.31/0.36	0.22	0.25
Winter 2003–2004	**1 Oct'03–12 April'02**								
Gore Pt.	0.61/0.61	0.19	0.00						
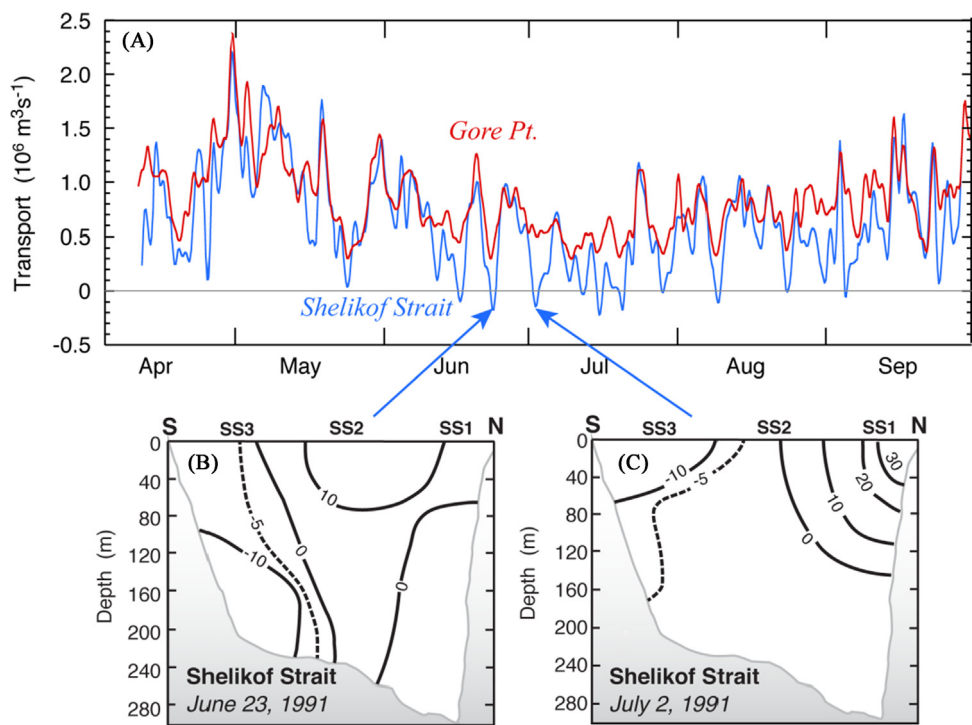
Fig. 7. (A) Time series of net transport at Shelikof Strait (blue) and Gore Point (red) for 1991. Cross sectional velocity (cm s^{-1}) at exit of Shelikof Strait for (B) June 23 and (C) July 2. Velocities are perpendicular to the plane of the moorings with positive into the page (southwestward) and negative out of the page (northeastward).

These waves were evident each year at GAK2 and GAK3, beginning in July or August and persisted into autumn, and sometimes into winter (e.g. 2013, Fig. 12). The signal was strongest at ~2 d, but a significant increase in energy extended to ~4 d in 2001 and 2003. The timing of these waves coincided with the seasonal increase in freshwater outflow from rivers, which occurs in August (Royer, 1982; Weingartner et al., 2005).

These meanders are one possible explanation for the poor correlations between the transport at Seward and those measured at the other mooring lines, and between the transport at Seward
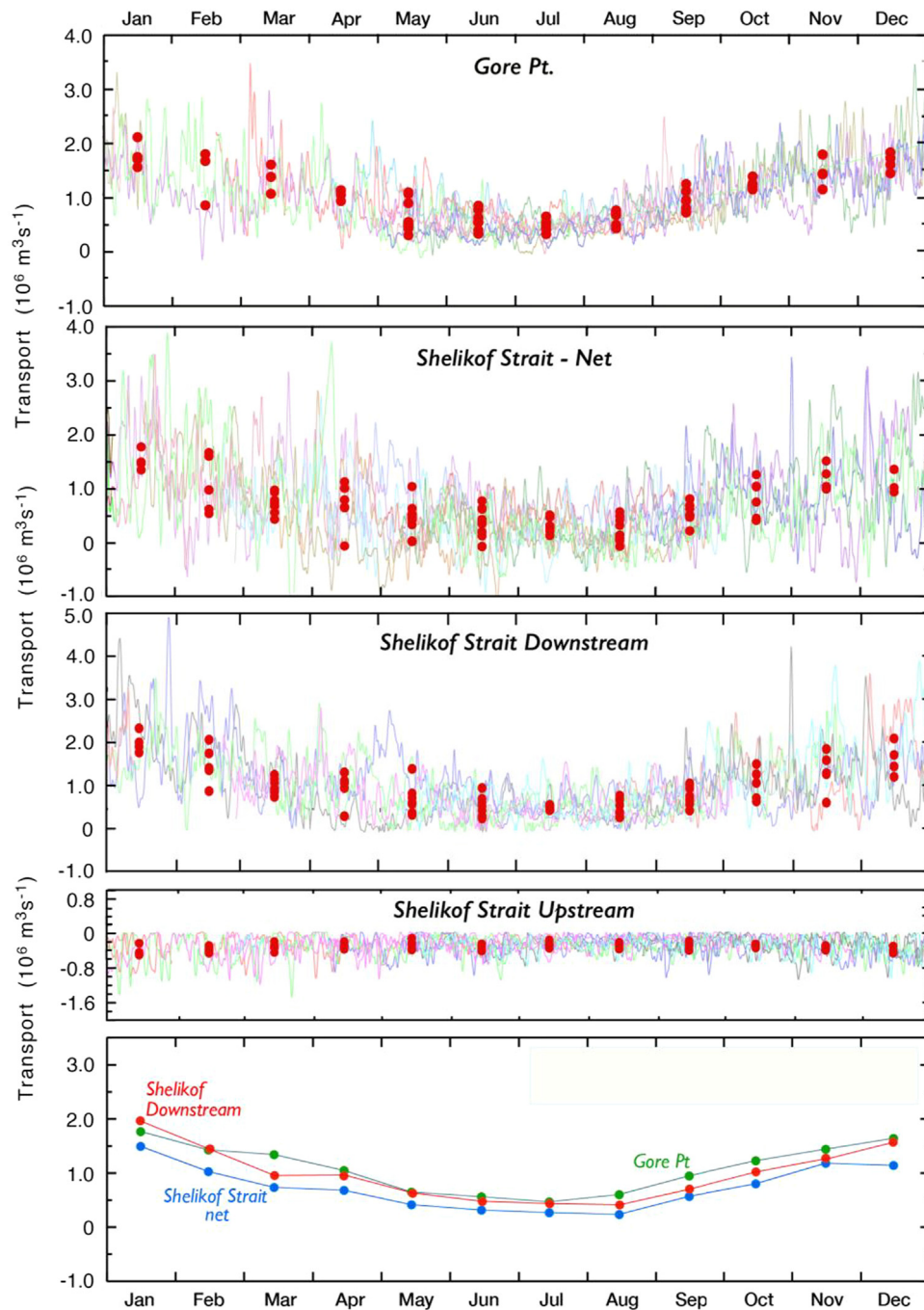
Fig. 8. Time series of transport at (A) Gore Point, (B) net transport at Shelikof Strait, (C) ACC transport at Shelikof Strait and (D) the upstream transport at Shelikof Strait exit. Each time series is shown muted in the background and the red dots are the monthly averages. (E) The annual signal (average of the individual monthly averages) for Gore Point (green), net Shelikof Strait (blue) and ACC Shelikof (red).

and the along-shore winds (Tables 1 and 3). Such waves may cause enhanced flow near GAK4 (and thus an under-estimation of the calculated transport) or even a partial interruption in transport. The lack of velocity measurements at GAK4 in 2001–2004 precluded examination of this hypothesis.

3.5. Bottom salinity signal in long-term records

In addition to a well-defined surface flow, the ACC, together with flow in the canyons and troughs, plays an important role in vertical and horizontal mixing of water. Stabeno et al. (2004) commented that the strong flow of the ACC through Kennedy

Entrance results in deep mixing, introducing salt (including nutrients) to surface waters and heat to near bottom water. Two long-term moorings, one at GAK1 and the second (CB1) in a bay near the Port of Kodiak on Kodiak Island provide insight into the impact of mixing on the bottom temperature and salinity in the northern GOA. The bottom moorings are at similar depths – 250 m at GAK1 and 200 m at CB1.

The annual temperature and salinity cycles at the long-term moorings at Seward (GAK1) and at the head of Chiniak Trough (CB1) are markedly different (Fig. 13A, B). The weak annual temperature signal at GAK1 has a maximum in early winter and a minimum in spring, while the larger signal at CB1 has a maximum

in September and a minimum in March, very similar to the timing of the seasonal surface signal (Stabeno et al., 2004). That the temperature at CB1 is approximately in phase with the near-surface ocean temperature indicates that strong surface-to-bottom mixing occurs throughout the year. In contrast, at GAK1 heat is deeply mixed only in the winter, when stratification weakens and winds intensify (Janout et al., 2010). Major mixing on the shelf of the northern GOA likely occurs on the banks (Cheng et al., 2012) and in regions of strong currents (including tides) such as Kennedy Entrance (Stabeno et al., 2004).

The stronger salinity signal was at GAK1, with lowest near-bottom salinities occurring in March, which is indicative of downward mixing of surface water primarily during winter. Higher salinities in summer were coincident with relaxation of downwelling, and the deep intrusion of saltier water onto the shelf (Ladd et al., 2005a). The weaker salinity signal at CB1 was freshest in early September (in phase with freshening of the surface),
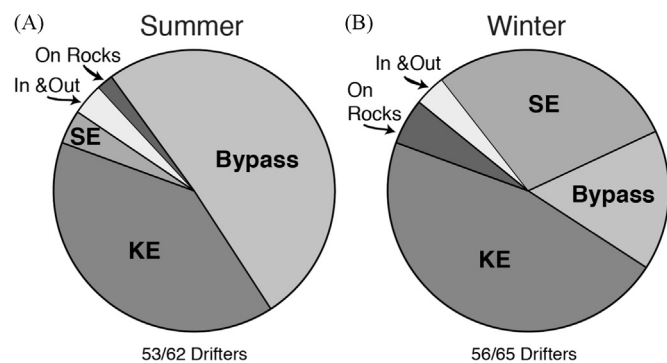

Fig. 9. The fate of drifters entering the box bounded by the Gore Point and Kennedy–Stevenson lines (Fig. 1-inset): passing through Kennedy Entrance (KE); Stevenson Entrance (SE); grounding out on rocks; passing through to Shelikof Strait and then reversing course (in and out); or bypassing the entrances as they are carried south around Kodiak Island. Two periods are considered: (A) summer, (B) winter. Each drifter is in one and only one category.

supporting the conclusion derived from the temperature time series that strong vertical mixing occurred throughout the year.

Even though the phase of the annual temperature signals differed markedly between these two long-term deep measurements, the temperature anomalies (temperature time series minus the annual signal in Fig. 13B) appeared related at low frequency (C). The monthly averaged time series anomaly at the two sites are correlated at $r=0.65$, with GAK1 lagging CB1 by two months. Not unexpectedly, both monthly mean temperature anomalies, in turn, were well correlated with the Pacific Decadal Oscillation (PDO), with the PDO signal leading the monthly mean temperature anomaly at CB1 (GAK1) by 1 (4) months with a correlation of 0.52 (0.38). That the monthly anomalies in temperature at CB1 lead those at GAK1 is a result of mixing of warm surface waters to depth at CB1. Thus, the surface temperature signal arrives at depth first at CB1 and later at GAK1.

3.6. Implications of mixing

A composite image of ocean color in August 2002–2011 (Fig. 14) shows higher concentrations of chlorophyll-a during summer surrounding Kodiak Island relative to other shelf waters in the GOA. On average, the highest chlorophyll concentrations appeared to be centered over and near the shallow banks south and east of Kodiak Island and in Shelikof Strait, with lower concentrations in the troughs and along the Kenai Peninsula, consistent with modeled results (Coyle et al., 2012; Cheng et al., 2012). These persistent features of increased summer chlorophyll concentrations can be interpreted as regions of higher primary production (Behrenfeld and Falkowski, 1997), where new production was sustained throughout the summer. Note the signals in upper Cook Inlet and in some coastal bays along the Alaska Peninsula are likely related to suspended sediment. To sustain new production, effective mechanisms of cross-shelf and/or vertical exchange must be operative, introducing nutrient-rich water into the euphotic zone of the shelf adjacent to Kodiak Island.
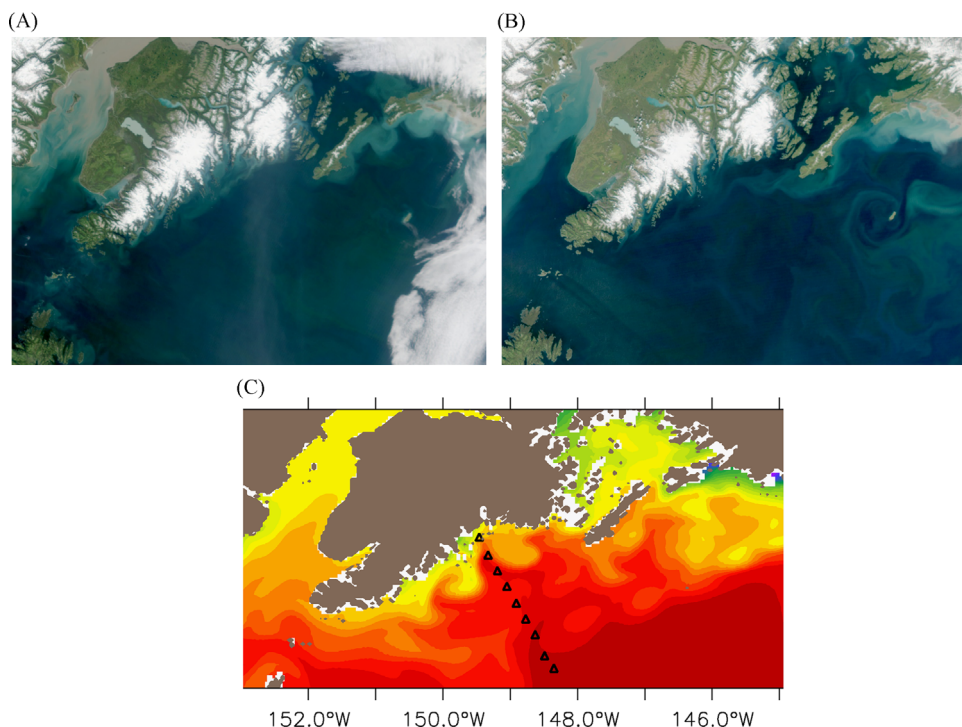

Fig. 10. True color satellite images for (A) August 22, 2001 and (B) September 3, 2002. (C) Modeled 5-m salinity on September 10, 2001. Triangles mark stations on the Seward line.
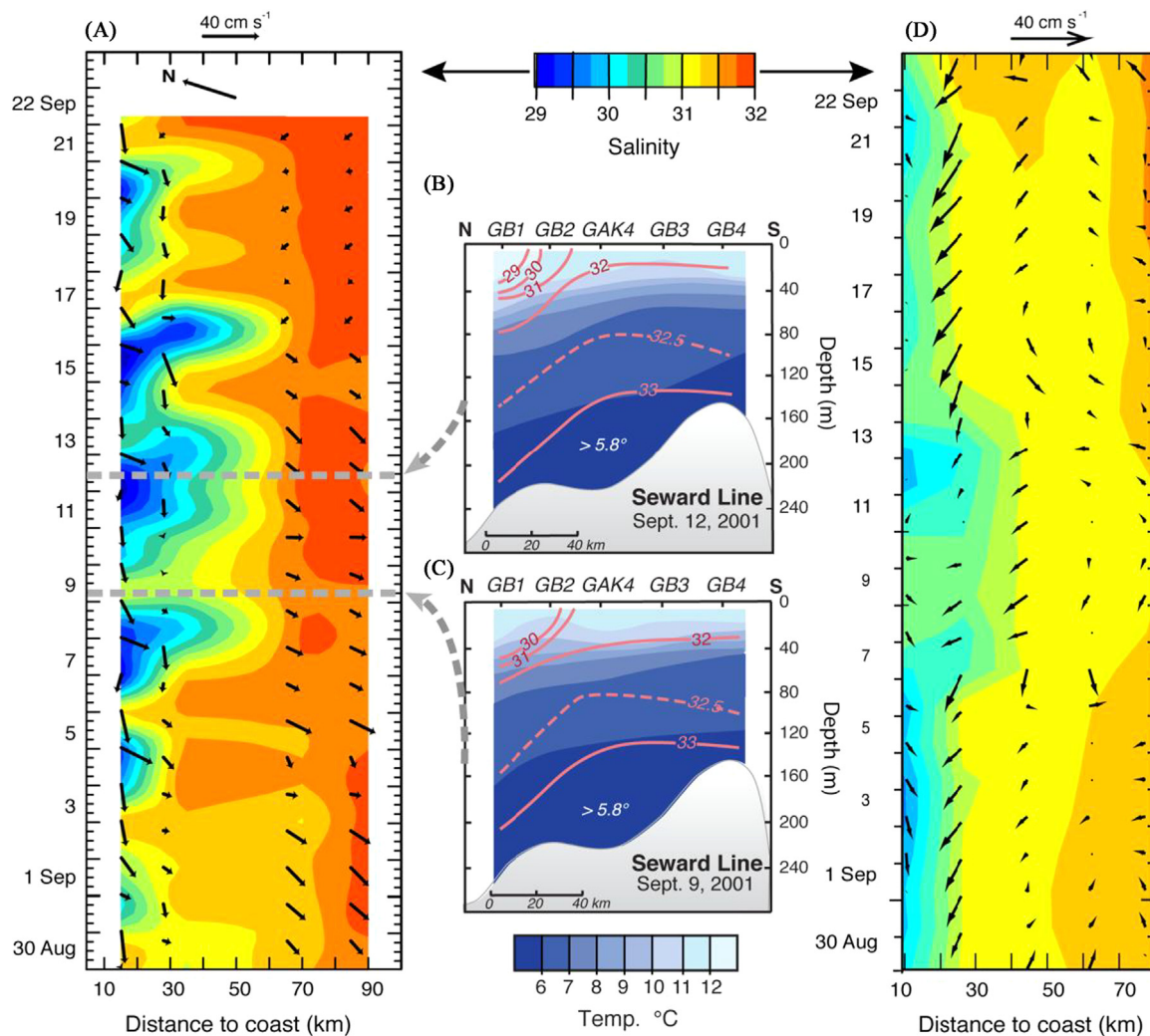
Fig. 11. (A) Time series of observed near-surface salinity (15–20 m) across the Seward line in 2001. The vectors are daily currents (from low pass filtered time series). (B) Observed vertical structure of temperature (blue fill) and salinity (red) contours centered on 9 September 0600 GMT and (C) 12 September 1200 GMT. (D) Modeled salinity at 5 m depth for the same time period.

The high chlorophyll concentrations in Shelikof Strait are likely a result of the strong tidal mixing in Kennedy Entrance, which vertically mixes the water column (Stabeno et al., 2004). Nutrients are mixed into the euphotic zone throughout the summer, and that water is then advected southwestward down Shelikof Strait where it supports a phytoplankton bloom. In addition, some (~10%) of the drifters that entered Kennedy Entrance then exited through Stevenson Entrance. This increase in nutrient availability in euphotic zone could contribute to the higher chlorophyll concentrations to the south of Stevenson Entrance, although mixing on banks are likely more important (Cheng et al., 2012).

During summer, approximately ~38% of the water which flows past Gore Point entered neither Kennedy nor Stevenson Entrance, but turned southward along the coast of Kodiak Archepelago. During summer, the water at Gore Point was largely unmixed, but data collected in Chiniak Trough indicated strong mixing occurs in the trough and over the banks to the southeast of Afognak Island (Ladd et al., 2005a). The salinity and temperature signals at CB1 also suggest that strong mixing occurred in this region. This mixing introduces nutrients into euphotic zone which would support prolonged production throughout the summer on the shelf around Kodiak Island. The record at GAK1 supports the premise that vertical mixing is weaker along the Kenai Peninsula, thus resulting in more limited summer production.

4. Summary and conclusions

The ACC is marked by strong spatial and temporal variability. Transport varies seasonally, with the strongest flow in late fall and winter and the weakest in summer. The transports at Gore Point, Kennedy–Stevenson Entrances and the exit to Shelikof Strait are largely controlled by along-shore winds. Model results show that an increase in freshwater does not result in a significant increase in the transport of the ACC (Hermann and Stabeno, 1996).

While winds largely control the transport of the ACC, freshwater input controls its vertical structure and is the major cause of the 2–6 day waves that occur both in Shelikof Strait and near Seward. These waves are likely one of the causes of the poor correlations between the transport at Seward and those at Gore Point, Kennedy–Stevenson and the exit to Shelikof Strait. Another cause may be the influence of gap winds, which have little impact on the transport at Seward, but can modify the transport at the Kennedy–Stevenson Entrances by as much 0.4×10^6 m^3 s^{-1} (Fig. 11 in Ladd et al., 2016) and the other two lines by a lesser amount. While gap wind events persist for relatively short periods of time, they drive intense surface processes during those intervals. Finally, the complexity of the bathymetry downstream from the Seward can also influence the currents.
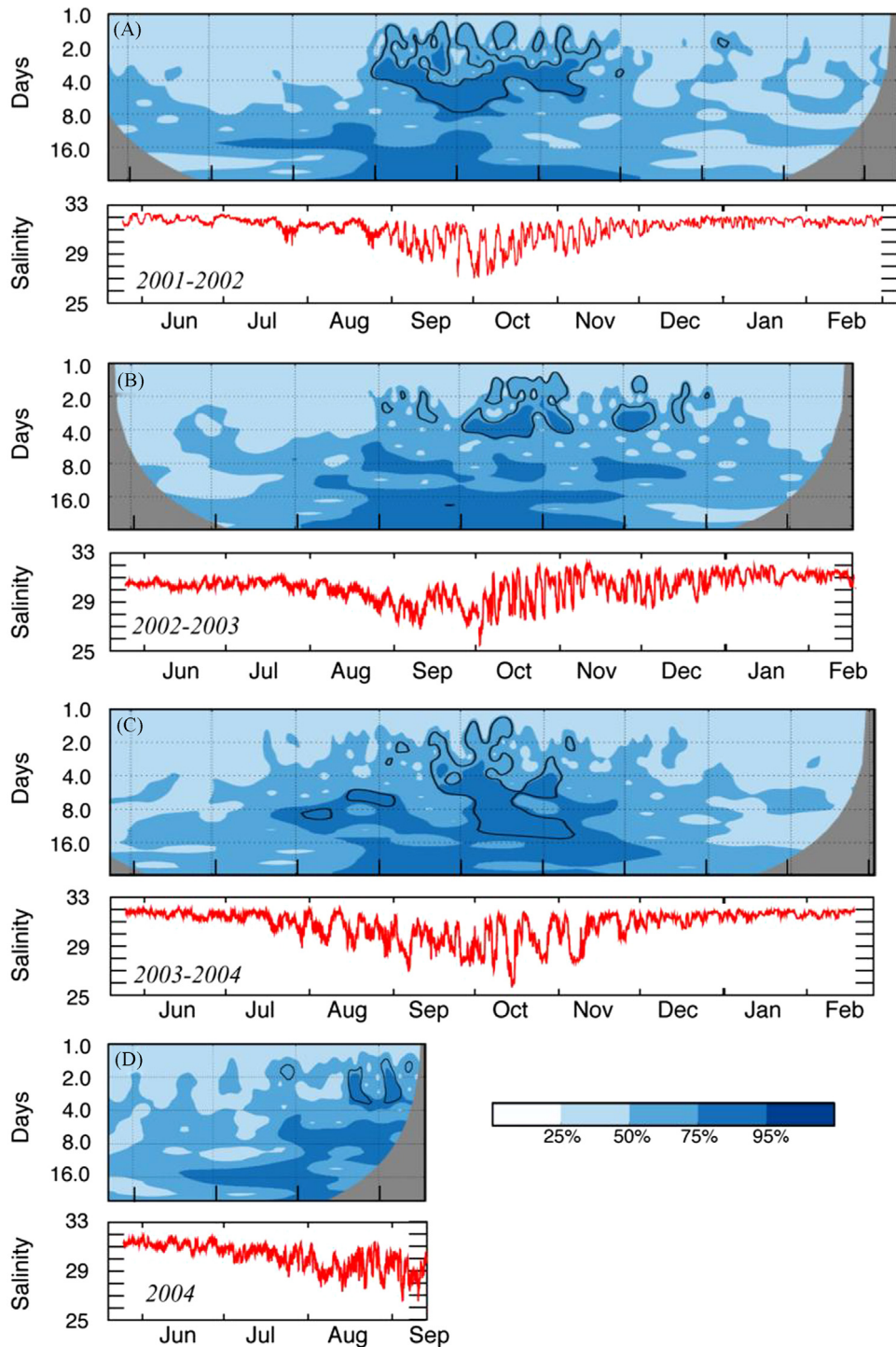
Fig. 12. Wavelet power spectrum of salinity at GAK2 from May 25 to the end of record for each year (A) 2001–2002, (B) 2002–2003, (C) 2003–2004, (D) summer 2004. "Scales" are comparable to Fourier time periods in days. Contour intervals were chosen such that the indicated percentage falls below the power level contoured (e.g. 25% of the data falls below the first level contoured). The thick contour denotes the 95% confidence level against a red noise spectrum and the gray region denotes the "cone of influence" where edge effects become important.

Vertical mixing plays an important role in summer in introducing nutrients into the euphotic zone and supporting prolonged summer production around Kodiak Island. Strong tidal mixing in Kennedy Entrance introduces the nutrients to the surface which are then advected southwestward down Shelikof Strait by the ACC, thereby supporting summer phytoplankton blooms in the strait. In contrast, the higher production to the south of Kodiak Island

appears to be related more to mixing over the banks and at their edges (Cheng et al., 2012).

The largest transport in the ACC was measured at Gore Point. It varies seasonally, with mean winter transport at Gore Point $\sim 1.4 \times 10^6$ m^3 s^{-1} and summer transport $\sim 0.6 \times 10^6$ m^3 s^{-1}. Using this as the reference, a schematic of relative transports along the 1700-km pathway from Seward to the eastern Aleutian Passes
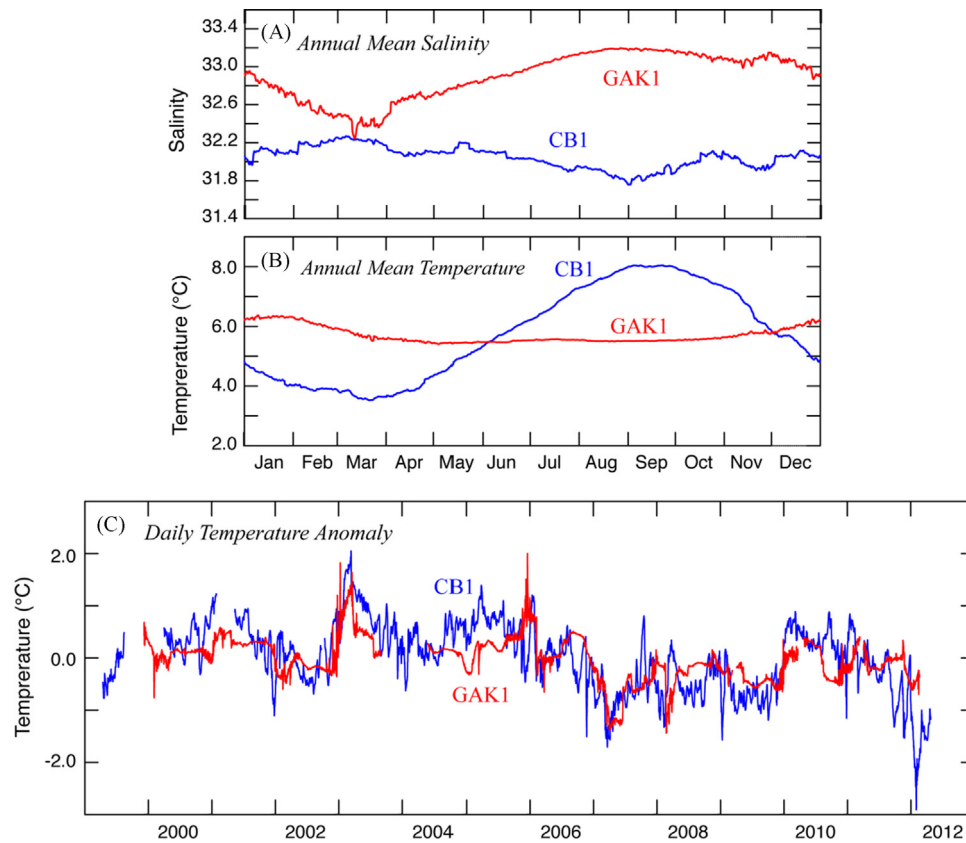
Fig. 13. The annual near-bottom (A) salinity and (B) temperature CB1 at Chiniak Bay (200 m) and GAK1 at Seward (250 m). (C) Temperature anomalies (6-hourly time series minus the annual temperature signals shown in B).
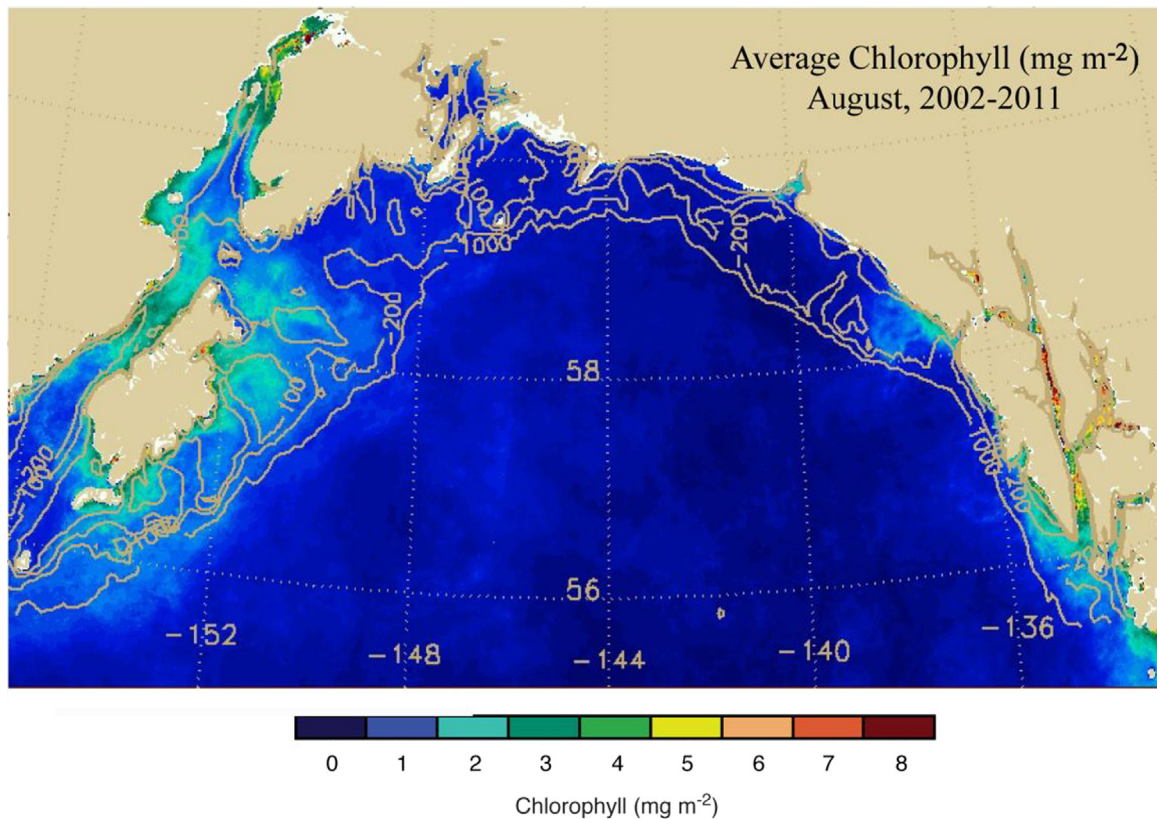

Fig. 14. SeaWiFS chlorophyll averaged between June 1 and August 31 for 1998–2002 showing the high, sustained productivity that takes place around Kodiak Island.
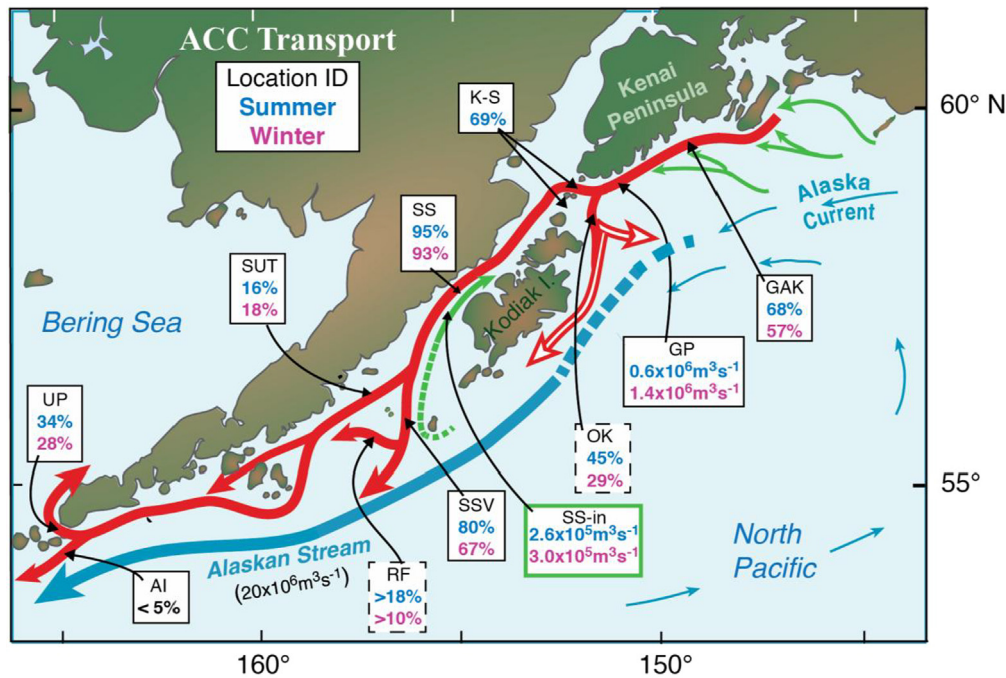
Fig. 15. Composite map of transport in the various branches of the ACC from Kayak Island to the Aleutian Islands. The hollow arrows are extrapolated pathways of the ACC. The thin green lines indicate likely contributions to the ACC in the east and measured upstream flow in Shelikof Strait. The highest mean transport was measured at Gore Point. The other squares indicate the percent of transport at Gore Point (GP) that occurs on each branch. The magnitude of inflow in Shelikof Strait is also given (green box). The transports at the exit to Shelikof Strait (SS), Kennedy–Stevenson Entrances (K–S), south side of Kodiak Archipeligo (OK) and Seward (GAK) are from this paper. The estimate of transport between Sutwik and the Semidi Islands (Sut) and between the Semidi Islands and Chirikof Islands (SSV) are from Schumacher et al. (1989). The flow through Unimak Pass (UP) is from Stabeno et al. (in press) and the Aleutian Islands (AI) continuation is estimated from Stabeno et al. (2005).

can be derived (Fig. 15). The composite velocity vectors derived from the drifter trajectories (Fig. 4) shows the ACC beginning to reform along Montigue Island. This is supported by modeling work of Wang et al. (2014). The transport at Gore Point is the combined flow at Seward and the westward flow on the north side of Amatuli Trough which originated at the slope. This onshore flow is likely an important source for nutrients for the region around Kodiak Island. While approximately a third (38% in summer and 29% in winter) of the transport at Gore Point flows southward along the east coast of the Kodiak Archipeligo, its exact pathway is unclear (open arrows). The composite vectors from the drifter trajectories (Fig. 4) indicate weak offshore flow on the south side of Amatuli Trough and alongshore flow on the south side of the Kodiak Archipelago. Approximately two-thirds of the Gore Point transport flows down Shelikof Strait past Cape Kekurnoi. The inflow up the Shelikof Sea Valley introduces $\sim 0.3 \times 10^6 \, \text{m}^3 \, \text{s}^{-1}$ into Shelikof Strait. This is entrained into the ACC, increasing the total outflow to $0.9 \times 10^6 \, \text{m}^3 \, \text{s}^{-1}$, slightly less than the transport at Gore Point.

The remainder of the current schematic (Fig. 15) is derived from previous research. After exiting Shelikof Strait $\sim 75\%$ of the ACC flows down the sea valley between Chirikof and Semidi Islands, while the remainder continues along the Alaska Peninsula eventually flowing between the Semidi Islands and Sutwik Island (Schumacher et al., 1989). There was only one year of data in that study, so the $75\% - 25\%$ ratio is used for both summer and winter. Individual drifter trajectories (not shown) indicate that the flow along the Alaska Peninsula bifurcates east of the Shumagin Islands (at 160°W) and rejoins to the west. The magnitude of flow through Unimak Pass is $0.2 \times 10^6 \, \text{m}^3 \, \text{s}^{-1}$ in summer and $0.4 \times 10^6 \, \text{m}^3 \, \text{s}^{-1}$ in winter (Stabeno et al., in press), while the flow through the other shallow passes west of Unimak Pass is weak (~ 0.1; Stabeno et al., 2005; Stabeno and Hristova, 2014). To balance the flow through the Aleutian Passes approximately a third of the flow

exiting the sea valley needs to return to the shelf in the shallow trough to the west of Shelikof Strait. Such a return flow is evident in the drifter composites (Fig. 4) and in individual drifter trajectories (not shown), but no moorings have deployed in that location so estimates of transport are not available.

The reliability of the transports depicted in Fig. 15 varies by location. The estimates of transport at Gore Point, the exit to Shelikof Strait and Unimak Pass all are derived from many years of observations. At Seward and Kennedy–Stevenson Entrances the observations are dominated by summer measurements. Probably the weakest estimates are derived from the single year of data which determines the split of the ACC in Shelikof Sea Valley. While the estimate of the magnitude of transport that flows southeast of Kodiak Archipelago is reliable, its pathways are largely inferred from drifters which provide little information of magnitude of transport or the flow in the bottom portion of the water column. Additional targeted measurements in the Shelikof Sea Valley and to the southeast of Kodiak would be useful, but likely not change the basic structure of this schematic.

References

Abookrie, A.A., Duffy-Anderson, J.T., Jump, C.M., 2005. Habitat associations and diet of young of the year Pacific cod near Kodiak Island, AK. Mar. Biol. 150, 713–726.

Behrenfeld, M.J., Falkowski, P.J., 1997. A consumer's guide to phytoplankton primary productivity models. Limnol. Oceanogr. 42, 1479–1491.

Brodeur, R.D., Wilson, M.T., 1996. Review of distribution, ecology, and population dynamics of age-0 walleye pollock in the Gulf of Alaska. Fish. Oceanogr. 5 (Supp. 1), S148–S166.

Carton, J.A., Geise, B.S., 2008. A reanalysis of ocean climate using Simple Ocean Data Assimilation (SODA). Mon. Weather. Rev. 136, 2999–3017. http://dx.doi.org/10.1175/2007MWR1978.1.

Chapman, D.C., 1985. Numerical treatment of cross-shelf boundaries in a barotropic coastal ocean model. J. Phys. Oceanogr. 15, 1060–1075.

Cheng, W., Hermann, A.J., Coyle, K.O., Dobbins, E.L., Kachel, N.B., Stabeno, P.J., 2012. Macro- and micro-nutrient flux to a highly productive submarine bank in the Gulf of Alaska: a model-based analysis of daily and interannual variability. Prog. Oceanogr. 101, 63–77. http://dx.doi.org/10.1016/j.pocean.2012.01.001.

Childers, A., Whitledge, T.E., Stockwell, D.A., 2005. Seasonal and interannual variability in the distribution of nutrients and chlorophyll-a across the Gulf of Alaska Alaska shelf: 1998–2000. Deep.-Sea Res. II 52, 193–216. http://dx.doi.org/10.1016/j.dsr2.2004.09.018.

Coyle, K.O., Cheng, W., Hinckley, S., Lessard, E.J., Whitledge, T., Hermann, A.J., Hedstrom, K., 2012. Model and field observations of effects of circulation on the timing and magnitude of nitrate utilization and production on the northern Gulf of Alaska shelf. Prog. Oceanogr. 103, 16–41.

Coyle, K.O., Gibson, G.A., Hedstrom, K., Hermann, A.J., Hopcroft, R.R., 2013. Zooplankton biomass, advection and production on the northern Gulf of Alaska shelf from simulations and field observations. J. Mar. Sys. 128, 185–207.

Curchitser, E.N., Haidvogel, D.B., Hermann, A.J., Dobbins, E.L., Powell, T.M., Kaplan, A., 2005. Multi-scale modeling of the North Pacific Ocean I: assessment and analysis of simulated basin-scale variability (1996–2003). J. Geophys. Res. 110, C11021. http://dx.doi.org/10.1029/2005JC002902.

Dai, A., Trenberth, K.E., 2002. Estimates of freshwater discharge from continents: latitudinal and seasonal variations. J. Hydrometeorol. 3, 660–687.

Doyle, M.J., Busby, M.S., Duffy-Anderson, J.T., Picquelle, S.J., Materese, A.C., 2002. Early life history of capelin in the northwest Gulf of Alaska: A historical perspective based on larval collections, October 1977–March 1979. ICES J. Mar. Sci. 59, 997–1005.

Durski, S.M., Glenn, S.M., Haidvogel, D.B., 2004. Vertical mixing schemes in the coastal ocean: comparison of the level 2.5 Mellor-Yamada scheme with an enhanced version of the K profile parameterization. J. Geophys. Res. 109, C01015. http://dx.doi.org/10.1029/2002JC001702.

Fairall, C.W., Bradley, E.F., Rogers, D.P., Edson, J.B., Young, G.S., 1996. Bulk parameterization of air-sea fluxes for Tropical Ocean-Global Atmosphere Coupled-Ocean Atmosphere Response Experiment. J. Geophys. Res. 101 (C2), 3747–3764. http://dx.doi.org/10.1029/95JC03205.

Favorite, F., Ingraham Jr., W.J., 1977. On flow in the northwestern Gulf of Alaska, May 1972. J. Oceanogr. Soc. Jpn. 33, 67–81.

Flather, R.A., 1976. A tidal model of the north-west European continental shelf. Mem. Soc. R. Sci. Liege 10, 141–164.

Foreman, M.G.G., Crawford, W.R., Cherniawsky, J.Y., Henry, R.F., Tarbotton, M.R., 2000. A high-resolution assimilating tidal model for the northeast Pacific Ocean. J. Geophys. Res. 105 (C12), 28629–28651. http://dx.doi.org/10.1029/1999JC000122.

Haidvogel, D.B., Arango, H.G., Hedstrom, K., Beckmann, A., Malanotte-Rizzoli, P., Shchepetkin, A.F., 2000. Model evaluation experiments in the North Atlantic Basin: simulations in nonlinear terrain-following coordinates. Dyn. Atmos. Ocean. 32, 239–281.

Haidvogel, D.B., Arango, H., Budgell, W.P., Cornuelle, B.D., Curchitser, E., Di Lorenzo, E., Fennel, K., Geyer, W.R., Hermann, A.J., Lanerolle, L., Levin, J., McWilliams, J.C., Miller, A.J., Moore, A.M., Powell, T.M., Shchepetkin, A.F., Sherwood, C.R., Signell, R.P., Warner, J.C., Wilkin, J., 2008. Ocean forecasting in terrain-following coordinates: formulation and skill assessment of the Regional Ocean Modeling System. J. Comput. Phys. 227, 3595–3624.

Hermann, A.J., Stabeno, P.J., 1996. An eddy-resolving model of circulation on the western Gulf of Alaska shelf: 1. Model development and sensitivity analyses. J. Geophys. Res. 101, 1129–1149.

Hermann, A.J., Curchitser, E.N., Haidvogel, D.B., Dobbins, E.L., 2009a. A comparison of remote vs. local influence of El Niño on the coastal circulation of the northeast Pacific. Deep.-Sea Res. II 56, 2427–2443. http://dx.doi.org/10.1016/j.dsr2.2009.02.005.

Hermann, A.J., Hinckley, S., Dobbins, E.L., Haidvogel, D.B., Bond, N.A., Mordy, C., Kachel, N., Stabeno, P.J., 2009b. Quantifying cross-shelf and vertical nutrient flux in the Gulf of Alaska with a spatially nested, coupled biophysical model. Deep.-Sea Res. II 56, 2474–2486.

Hollowed, A.B., Wilson, C.D., Stabeno, P.J., Salo, S.A., 2007. Effect of ocean conditions on the cross-shelf distribution of walleye pollock (Theragra chalcogramma) and capelin (Mallotus villosus). Fish. Oceanogr. 16, 142–154. http://dx.doi.org/10.1111/j.1365-2419.2006.00418.x.

Hsu, S.A., Meindl, E.A., Gilhousen, D.B., 1994. Determining the power-law windprofile exponent under near-neutral stability conditions at sea. J. Appl. Meteor 33, 757–765.

Janout, M.A., Weingartner, T.J., Royer, T.C., Danielson, S.L., 2010. On the nature of winter cooling and the recent temperature shift on the northern Gulf of Alaska shelf. J. Geophys. Res. 115, C05023. http://dx.doi.org/10.1029/2009JC005774.

Kalnay, E., Kanamitsu, M., Kistler, R., Collins, W., Deaven, D., Gandin, L., Iredell, M., Saha, S., White, G., Woollen, J., Zhu, Y., Leetmaa, A., Reynolds, R., Chelliah, M., Ebisuzaki, W., Higgins, W., Janowiak, J., Mo, K.C., Ropelewski, C., Wang, J., Jenne, R., Joseph, D., 1996. The NCEP/NCAR 40-Year Reanalysis Project. Bull. Am. Meteor. Soc. 77, 437–471. http://dx.doi.org/10.1175/1520-0477(1996)077 < 0437:TNYRP > 2.0.CO;2.

Kundu, P., Allen, J., 1976. Some three dimensional characteristics of low-frequency current fluctuations near the Oregon coast. J. Phys. Oceanogr. 6, 181–199.

Ladd, C., Bond, N.A., 2002. Evaluation of the NCEP/NCAR reanalysis in the NE Pacific and the Bering Sea. J. Geophys. Res. 107 (C10), 3158. http://dx.doi.org/10.1029/2001JC001157.

Ladd, C., Stabeno, P.J., Cokelet, E.D., 2005a. A note on cross-shelf exchange in the northern Gulf of Alaska. Deep.-Sea Res. II 52, 667–679.

Ladd, C., Kachel, N.B., Mordy, C.W., 2005b. Observations from a Yakutat eddy in the northern Gulf of Alaska. J. Geophys. Res. 110, C03003.

Ladd, C., Mordy, C.W., Kachel, N.B., Stabeno, P.J., 2007. Northern Gulf of Alaska eddies and associated anomalies. Deep.-Sea Res. I 54, 487–509.

Ladd, C., Cheng, W., Salo, S., 2016. Gap Winds near Kodiak Island, Alaska and effects on regional oceanography. Deep-Sea Res. II 132, 54–67. http://dx.doi.org/10.1016/j.dsr2.2015.08.005.

Large, W., McWilliams, J., Doney, S., 1994. Oceanic vertical mixing: a review and a model with a non-local boundary layer parameterization. Rev. Geophys. 32, 363–403.

Marchesiello, P., McWilliams, J.C., Shchepetkin, A.F., 2001. Open boundary conditions for long-term integration of regional oceanic models. Ocean. Model. 3, 1–20.

Mesinger, F., DiMego, G., Kalnay, E., Mitchell, K., Shafran, P.C., Ebisuzaki, W., Jovic, D., 2006. North American regional reanalysis. Bull. Am. Meteorol. Soc. 87 (3), 343–360. http://dx.doi.org/10.1175/BAMS-87-3-343.

Meuter, F.J., Norcross, B.L., 2002. Spatial and temporal patterns in the demersal fish community on the shelf and upper slope regions of the Gulf of Alaska. Fish. Bull. 100, 559–581.

Musgrave, D.L., Halverson, M.J., Pegau, S.W., 2013. Seasonal surface circulation, temperature, and salinity in Prince William Sound, Alaska. Cont. Shelf Res. 53, 20–29. http://dx.doi.org/10.1016/j.csr.2012.12.001.

Mysak, L.A., Muench, R.D., Schumacher, J.D., 1981. Baroclinic instability in a downstream varying channel: Shelikof Strait, Alaska. J. Phys. Oceanogr. 11, 950–969.

Niebauer, H.J., Royer, T.C., Weingartner, T.J., 1994. Circulation of Prince William Sound, Alaska. J. Geophys. Res 99 (C7), 14113–14126. http://dx.doi.org/10.1029/94jc00712.

Reed, R.K., Schumacher, J.D., 1986. Physical oceanography. In: Hood, D.W., Zimmerman, S.T. (Eds.), The Gulf of Alaska: Physical Environment and Biological Resources. U.S. Department of Commerce and U.S. Department of the Interior, pp. 57–75.

Royer, T.C., 1981. Baroclinic transport in the Gulf of Alaska. Part II. Fresh water driven coastal current. J. Mar. Res. 39, 251–266.

Royer, T.C., 1982. Coastal freshwater discharge in the northeast Pacific. J. Geophys. Res. 87 (C3), 22017–22021. http://dx.doi.org/10.1029/JC087iC03p2017.

Royer, T.C., Grosch, C.E., 2007. Update of freshwater discharge model for Gulf of Alaska. North Pacific Research Board Final Report, NPRB Project 734, 12 pp.

Schumacher, J.D., Stabeno, P.J., Roach, A.T., 1989. Volume transport in the Alaska Coastal Current. Cont. Shelf Res. 9, 1071–1083.

Shchepetkin, A.F., McWilliams, J.C., 1998. Quasi-monotone advection schemes based on explicit locally adaptive dissipation. Mon. Weather. Rev. 126, 1541–1580.

Shchepetkin, A.F., McWilliams, J.C., 2003. A method for computing horizontal pressure-gradient force in an oceanic model with a nonaligned vertical coordinate. J. Geophys. Res. 108 (C3), 3090. http://dx.doi.org/10.1029/2001JC001047.

Shchepetkin, A.F., McWilliams, J.C., 2005. The regional oceanic modeling system (ROMS): a split-explicit, free-surface, topography-following-coordinate oceanic model. Ocean. Model. 9, 347–404. http://dx.doi.org/10.1016/j.ocemod.2004.08.002.

Stabeno, P.J., Hristova, H.G., 2014. Observations of the Alaskan Stream near Samalga Pass and its connection to the Bering Sea: 2001–2004. Deep.-Sea Res. I 88, 30–46. http://dx.doi.org/10.1016/j.dsr.2014.03.002.

Stabeno, P.J., Reed, R.K., 1994. Circulation in the Bering Sea basin observed by satellite-tracked drifters: 1986–1993. J. Phys. Oceanogr. 24, 848–854.

Stabeno, P.J., Reed, R.K., Schumacher, J.D., 1995. The Alaska Coastal Current: continuity of transport and forcing. J. Geophys. Res. 100, 2477–2485.

Stabeno, P.J., Bond, N.A., Hermann, A.J., Kachel, N.B., Mordy, C.W., Overland, J.E., 2004. Meteorology and oceanography of the northern Gulf of Alaska. Cont. Shelf Res. 24, 859–897.

Stabeno, P.J., Kachel, D.G., Kachel, N.B., Sullivan, M.E., 2005. Observations from moorings in the Aleutian Passes: Temperature, salinity and transport. Fish. Oceanogr. 14 (Suppl. 1), S39–S54. http://dx.doi.org/10.1111/j.1365-2419.2005.00362.x.

Stabeno, P.J., Bond, N.A., Kachel, N.B., Ladd, C., Mordy, C.W., Strom, S.L., 2016. Southeast Alaska: currents, mixing and chlorophyll-a. Deep.-Sea Res. II 132, 6–23. http://dx.doi.org/10.1016/j.dsr2.2015.06.018.

Stabeno, P.J., Danielson, S., Kachel, D., Kachel, N.B., Mordy, C.W., 2016b. Currents and transport on the eastern Bering Sea shelf. Deep.-Sea Res. II (in press).

Strom, S.L., Olson, M.B., Macri, E.L., Mordy, C.W., 2007. Cross-shelf gradients in phytoplankton community structure, nutrient utilization, and growth rate in the coastal Gulf of Alaska. Mar. Ecol. Prog. Ser. 328, 75–92.

Wang, Y., Xue, H., Chai, F., Chao, Y., Farrara, J., 2014. A model study of the Copper River plume and its effects on the northern Gulf of Alaska. Ocean. Dyn. 64, 241–258. http://dx.doi.org/10.1007/s10236-013-0684-3.

Weingartner, T.J., Danielson, S.L., Royer, T.C., 2005. Freshwater variability and predictability in the Alaska Coastal. Curr. Deep.-Sea Res. II 52, 169–191.

Wilson, M.T., 2000. Effects of year and region on the abundance and size of age-0 walleye pollock, *Theragra chalcogramma*, in the western Gulf of Alaska, 1985–1988. Fish. Bull. 98, 823–834.